ChemComm

HIGHLIGHT

View Article Online
View Journal | View Issue

Cite this: *Chem. Commun.*, 2025, **61**, 3582

Proton-conducting copper-based MOFs for fuel cells

Byong June Kim, [a] Sun Ho Park, [a] Mariana L. Díaz-Ramírez [ab] and Nak Cheon Jeong *[ab]

Metal–organic frameworks (MOFs) are emerging as promising alternatives for proton-conductive materials due to their high porosity, large surface area, stability, and relatively low cost. Among these, copper-based MOFs (Cu-MOFs) stand out with unique advantages, including open metal sites, variable valence states, and strongly electrophilic Cu centers. In this review, we discuss recent advances and developments in the use of Cu-MOFs as proton-conductive materials, with a particular focus on their application as proton exchange membranes (PEMs). We introduce the most common strategies employed to date and review the key features that have contributed to the construction of efficient proton transport pathways in Cu-MOFs. Additionally, we review PEMs fabricated *via* direct thin-film deposition or as mixed-matrix membranes (MMMs) incorporating Cu-MOF fillers. Finally, we address the challenges that must be overcome in the coming years to develop more robust Cu-MOFs and to create more efficient thin films and Cu-MOF-based MMMs.

Received 2nd December 2024,
Accepted 27th January 2025

DOI: 10.1039/d4cc06378c

rsc.li/chemcomm

1. Introduction

Fuel cells have garnered attention as advantageous energy conversion technologies due to their ability to convert chemical energy into electrical energy efficiently. Compared to combustion engines, fuel cells produce lower or even zero emissions of regulated pollutants. Consequently, they are considered for applications across diverse fields, including transportation,[1,2] distributed energy generation systems,[3–5] and portable electronic devices.[6,7] Among the fuel cell technologies currently developing, those utilizing solid-phase electrolyte membranes show the most promise. Proton-exchange membrane fuel cells (PEMFCs), which use H_2, methane, or methanol as fuel, are particularly prevalent due to their production of water vapor as the only byproduct. Direct methanol fuel cells (DMFCs), a subset of PEMFCs specifically using methanol as fuel, are especially suited for portable devices.[8,9]

The core of these fuel cell technologies is the proton-exchange membrane (PEM), placed between two porous carbon-based electrodes that contain metal nanoparticles, such as platinum, which serve as catalysts for electrochemical reactions (see Fig. 1(a)). The primary function of the PEM is to facilitate proton transport from the anode to the cathode while electrons travel through an external circuit to the cathode.[10,11]

[a] *Department of Physics & Chemistry, DGIST, Daegu 42988, Korea. E-mail: nc@dgist.ac.kr*
[b] *Center for Basic Science, DGIST, Daegu 42988, Korea*

Byong June Kim

Byong June Kim received his BSc in 2020 from KAIST and is currently pursuing his PhD under the supervision of Prof. Nak Cheon Jeong. His research focuses on the diffusion and conductivity of metal–organic frameworks (MOFs).

Sun Ho Park

Sun Ho Park received his BSc in 2019 from DGIST and is currently pursuing his PhD under the supervision of Prof. Nak Cheon Jeong. His research focuses on the coordination chemistry of metal–organic frameworks (MOFs).

Two crucial properties of the PEM are paramount: (i) its ability to transport protonic species such as H^+, H_3O^+, and NH_4^+, which dictates proton conductivity (σ), depending largely on the concentration and mobility of proton carriers, and (ii) the activation energy (E_a) required for proton transport, which depends on the transport pathway. Depending on the magnitude of the activation energy, the proton transport mechanism can be classified into two categories: (i) the vehicle model, in which proton carriers move like vehicular entities with higher activation energy (>0.5 eV), and (ii) the Grotthuss model, characterized by lower activation energy (≤ 0.5 eV), where protons hop through hydrogen bonds (H-bonds).[12–14] The Grotthuss transport, generally conducted by H-bonds between the water molecules, is preferable since the low activation energy correlates with efficient proton conduction at low temperatures. Therefore, incremental water content in the PEM under low humidity conditions is one of the primary considerations for enhancing the performance of proton conductivity by forming H-bonds.

Among commercially available PEM materials, Nafion—a copolymer comprised of a hydrophobic backbone of perfluoroethylene with randomly distributed hydrophilic sulfonic acid groups—exhibits high proton conductivity (0.1 S cm^{-1}) at low temperatures.[15] Recently, several polymers, such as perfluorosulfonic acid (PFSA),[16] sulfonated polyphenylene (SPP),[17] and poly(2,3,5,6-tetrafluorostyrene-4-phosphonic acid),[18] with improved proton conductivity, mechanical strength, and temperature resistance have newly been developed. However, Nafion-based PEMs suffer from limitations such as excessive swelling and water loss at high temperatures, high production costs, and low durability, which have hindered their broader application in PEMFCs.[19,20] As a result, substantial research efforts have been directed toward exploring novel proton-conductive materials with superior proton transport capabilities.

Crystalline porous materials have attracted significant interest as promising candidates for proton-conducting applications. Metal–organic frameworks (MOFs), composed of metal ions or metal-oxo clusters coordinated with organic linkers, have emerged as particularly noteworthy materials for PEMs due to their ability to be precisely engineered to meet specific criteria for pore size and the chemical environment by selecting suitable metal ions[21,22] and organic linkers with appropriate lengths, bulkiness,[23] and functional groups.[24,25] Their substantial void spaces facilitate the incorporation of proton-conducting media such as water,[26] non-volatile acids,[27] and protic organic molecules or ions,[28,29] thereby enhancing conductivity. The high crystallinity of MOFs, characterized by long-range order, theoretically offers uninterrupted pathways for proton transport, which is crucial for understanding and modeling proton conduction mechanisms within porous materials.[30,31] Historically, after first reported by Kanda *et al.* in 1979,[32] the MOF proton conductivity has begun to be intensively studied with copper dithiooxamidate.[33] Then, the research has been broadly expanded to other MOFs comprised of various metal ions, such as zinc,[34] chromium,[35] cerium,[36] and iron,[37] giving rise to much progress on the topic. Nevertheless, we focus this review on the copper-based metal–organic frameworks (Cu-MOFs) due to Cu's natural abundance (60 ppm in Earth's crust),[38] its cost-efficiency, and Cu-MOFs' specific physicochemical features such as redox activity, high specific surface area, and, in certain instances, the potential presence of open metal sites.[39–42] These characteristics, combined with their structural diversity, have positioned Cu-MOFs as promising materials to use as PEMs in fuel cells.

Pioneering studies on Cu-containing proton-conductive coordination polymers, assembled with disubstituted dithiooxamide linkers, demonstrated proton conductivities ranging from 10^{-6} to 10^{-4} S cm^{-1} at 27 °C under water vapor-saturated air conditions.[43–45] In the study, it was postulated that an H-bonds network between free water molecules, nitrogen/sulfur atoms, and –OH groups within the MOF framework facilitated efficient proton conduction. Although these initial studies did not provide a comprehensive understanding of the proton transport mechanism, significant advancements have been made in the field of Cu-MOFs as proton conductors:

Mariana L. Díaz-Ramírez

Mariana L. Díaz-Ramírez was born and grew up in Mexico City. She received her PhD from UNAM (Mexico) in Materials Science and Engineering. She joined Prof. Jeong's group at DGIST (South Korea) in 2022. Her research interests include design and synthesis of nanoporous materials for applications such as gas adsorption and heterogeneous catalysis.

Nak Cheon Jeong

Nak Cheon Jeong is a Professor of Chemistry at DGIST, South Korea. He earned his PhD from Sogang University in 2008 and completed postdoctoral research at Northwestern University with Professor Joseph Hupp, focusing on metal–organic frameworks (MOFs) and solar energy. Since joining DGIST in 2012, his research has explored MOF chemistry, including catalysis, water stability, and sustainable materials. He has received accolades such as the Young Inorganic Chemist Award (2016) and the Excellent Inorganic Research Award (2024) from the Korean Chemical Society.

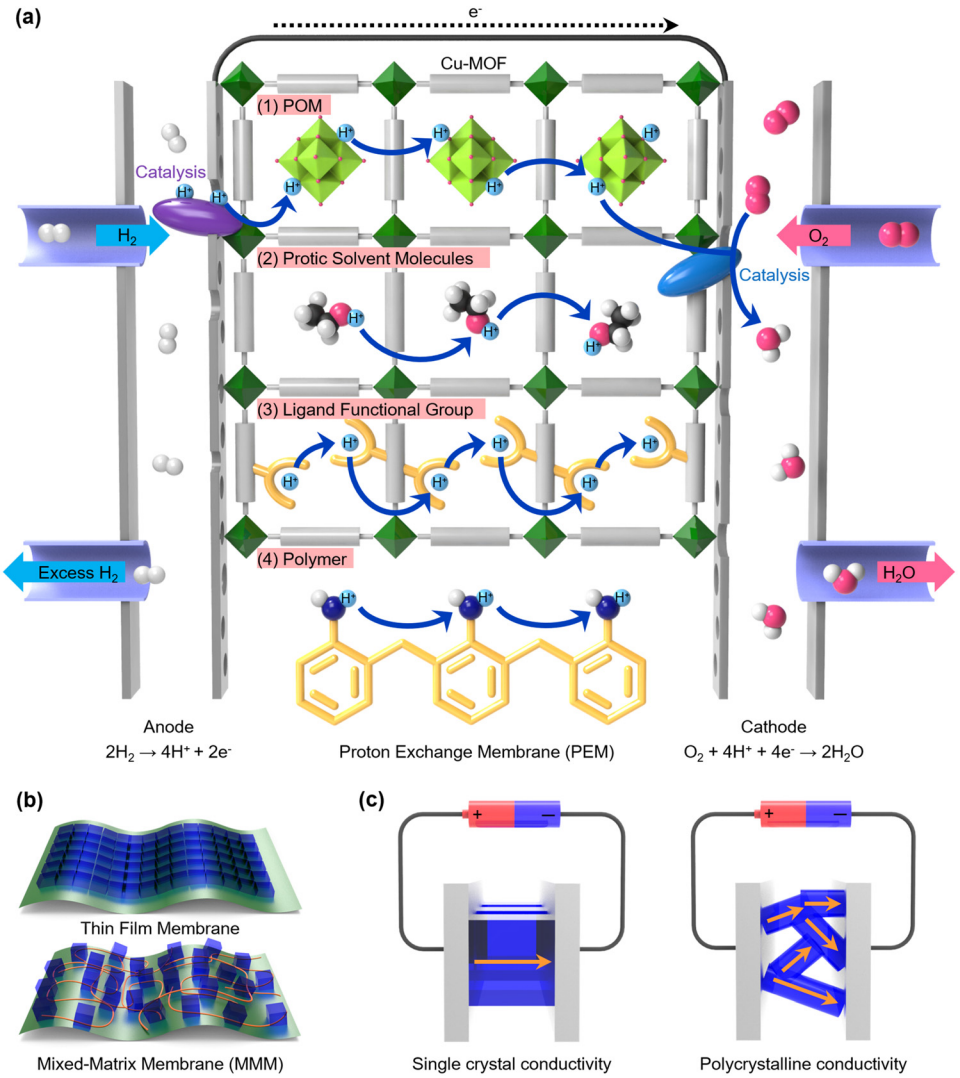

Fig. 1 (a) Fuel cell construction and proton transport strategies. Proton transportation can be designed in four different strategies: (1) introducing polyoxometalate (POM) in a pore or as a metal cluster, (2) coordinating protic solvent molecules with hydrogen bonds, (3) functionalizing the ligand which can form hydrogen bonds (nitrogen in azole) or acidic functional group which provides the proton (sulfonic acid or sulfonate group), and (4) incorporating polymer which has an acidic functional group such as sulfonated poly(ether ether ketone), SPEEK. (b) Proton exchange membrane (PEM) can be fabricated in two ways: thin film membrane and mixed-matrix membrane (MMM). (c) Thin film membrane conductivity is related to single-crystal conductivity, while mixed-matrix membrane stands for polycrystalline conductivity.

diverse functionalities have been incorporated to enhance proton transport capacity, highly stable frameworks have been engineered, and insights into conduction mechanisms have been partially elucidated.

This highlight aims to delineate the progress in leveraging Cu-MOFs as proton conductors for fuel cells, structured into two main sections. The first section focuses on single-crystalline and poly-crystalline Cu-MOFs and their efficacy as proton-conducting materials. This section is subdivided into four subsections based on the modifications made to enhance hydrophilicity and facilitate proton transport: (1) the incorporation of polyoxometalates (POMs) into the pores, (2) the inclusion of H-bond-forming guest molecules such as protic solvent molecules, (3) functionalization of organic linkers capable of forming H-bonds or containing acid groups, and (4) incorporating polymers with acidic functional groups, such as sulfonate poly(ether ether ketone) (see Fig. 1(a)).

While MOFs have shown potential as proton exchange membranes, their micron-scale sizes and brittleness present challenges for their industrial application. The second main section introduces the MOF fabrication methods with two strategies to overcome these challenges and thereby enhance the properties of fuel cell membranes (see Fig. 1(b)). (1) The first strategy involves growing Cu-MOFs as thin films on a membrane, which arranges proton conduction pathways and reduces grain boundaries—key obstacles to proton mobility. (2) The second strategy involves fabricating composite materials with proton-conductive polymers as mixed-matrix membranes (MMMs), providing proton transport pathways between MOF crystals through the polymer matrix. Each method relates to two

different approaches for measuring proton conductivity: single-crystalline conductivity and polycrystalline conductivity (see Fig. 1(c)). Single-crystalline conductivity provides an intrinsic property measured with an individual crystal, reflecting its inherent ability to conduct protons. By contrast, polycrystalline conductivity is measured after packing the crystals into a pellet, which differs from single-crystalline conductivity. Thus, distinguishing the conductivity based on the measurement method is crucial for evaluating their suitability as fuel cell membranes. The final section offers an overview of the findings and presents ideas and recommendations for advancing the development and understanding of these promising materials.

2. Proton conductivity in single- and poly-crystalline copper MOF

2.1. Polyoxometalate-incorporated MOFs

Polyoxometalates (POMs) are self-assembled polyatomic clusters containing transition metal oxo-anions with well-defined connectivity. Due to their oxygen-enriched surfaces, POMs can serve as relay centers in proton conduction, and their strong Brønsted acidity allows them to provide abundant protons readily.[46–48] However, the water solubility and structural instability of POMs hinder their direct use in proton-exchange membrane fuel cells (PEMFCs). Therefore, strategies that exploit their advantageous properties while improving their stability are required, such as immobilizing POMs in porous materials or constructing more stable frameworks using them.

One approach to enhance the stability of POMs is to use organic linkers that covalently or coordinatively bond with MOFs, serving as connecting agents instead of metal clusters. For example, using a Cu(II)-Schiff-base cation and a 1D chain $[Cu(DMF)_4(SiW_{12}O_{40})]_n^{2n-}$ to form a 3-dimensional network with hydrophilic cavities (see Fig. 2(a)).[49] This material exhibited moderate conductivity, reaching 5.94×10^{-4} S cm^{-1} at 100 °C under 98% RH, primarily due to constrained intergrain proton transfer. A previous study which exploits different strategies reported a Cu-MOF with polyoxomolybdate connecting nodes ($Cu_3Mo_5P_2$), where water molecules coordinated to the Cu center, forming a one-dimensional channel with a conductivity of 2.2×10^{-5} S cm^{-1} at 28 °C under 98% RH.[50] However, the conductivity decreased above 42 °C as water molecules were dislocated from the 1-D channel. Later, Keggin anions $[PM_{12}O_{40}]^{3-}$ (M = Mo or W) were employed as bidentate linkers to assemble Cu-MOFs based on 2,2′-bipyridyl-3,3′-dicarboxylic acid (H_2bpdc), specifically $[H\{Cu(Hbpdc)(H_2O)_2\}_2(PM_{12}O_{40})\cdot nH_2O]_n$, as reported by Duan and his group.[51] The resulting one-dimensional hydrophilic channels, lined with water molecules H-bonded to oxygen atoms of the polyanion or the H_2bpdc linkers, provided suitable pathways for proton conduction (Fig. 2(b)). The maximum conductivity for these materials, measured at 100 °C under 98% RH, was 1.25×10^{-3} S cm^{-1} for $[H\{Cu(Hbpdc)(H_2O)_2\}_2(PMo_{12}O_{40})\cdot nH_2O]_n$ and 1.56×10^{-3} S cm^{-1} for $[H\{Cu(Hbpdc)(H_2O)_2\}_2(PW_{12}O_{40})\cdot nH_2O]_n$, although the loss of water molecules above 100 °C caused a drop in conductivity of up to six orders of magnitude at 150 °C.

POMs as connecting agents for copper–pyridine complexes have also been investigated. Zhang and coworkers developed two POM-based frameworks: $H_2[Cu_2OL_3(H_2O)_2][Ce(L)(H_2O)_3(PW_{11}O_{39})]\cdot 17H_2O$ and $H_4[CuL_3]_2[Ln(H_2O)_3(PW_{11}O_{39})]_2\cdot 28H_2O$ (L = 4,4′-bipyridine).[52] These frameworks connect $[Ln(PW_{11}O_{39})]^{4-}$ with copper–bipyridine complexes, forming a 3D structure by stacking 2D layers (Fig. 2(c)). The proton conductivity increased from 3.255×10^{-6} S cm^{-1} to 3.175×10^{-4} S cm^{-1} as temperatures increased (Fig. 2(d)), with proton transport activation energy calculated as 1.445 eV at lower temperatures and 0.456 eV at higher temperatures than 55 °C. Both regions exhibited higher activation energy than 0.4 eV, indicating a vehicle-type proton transport mechanism, as the authors claimed. PXRD patterns demonstrated that the framework retained its structure even after exposure to humid conditions, supporting the notion that incorporating POM enhances stability.

Incorporating POMs as guest entities into MOF pores is another viable strategy to improve stability. Wei and colleagues reported the preparation of a proton-conducting MOF, $[\{Cu_4(dpdo)_{12}\}\{H(H_2O)_{27}(CH_3CN)_{12}\}\{PW_{12}O_{40}\}_3]_n$ (with dpdo = 4,4′-bipyridine-*N*,*N*′-dioxide), where $[PW_{12}O_{40}]^{3-}$ was hosted in the MOF cavities along with a large number of water molecules.[53] The material achieved a maximum conductivity of 1.25×10^{-4} S cm^{-1} at 100 °C under 98% RH, with an endothermic dissociation process of $H^+(H_2O)_{27}$ clusters yielding an activation energy of 0.82 eV. Lun and coworkers synthesized four polynuclear coordination polymers with POM coordination into the pores, one of which was a copper-based MOF with trinuclear $Cu_3(OH)$ subunits (Fig. 3(a) and (b)).[54] This Cu-MOF exhibited the highest proton conductivity with the value of 3.05×10^{-5} S cm^{-1} at 25 °C and 98% RH, with high thermal (retaining its structure up to 300 °C) and hydrolytic stability. By the way, increasing the temperature to 85 °C resulted in an increased proton conductivity with the value of 2.57×10^{-4} S cm^{-1}, and the subsequent incorporation of Nafion into the Cu-MOF under the same conditions further increased the conductivity up to 1.28×10^{-2} S cm^{-1}, implying that the synergetic interaction between MOFs and Nafion allows the formation of reconfigurable hydrogen bonds, which enhance proton transfer.

First envisioned as heterogeneous catalysts for hydrolysis of esters, Liu and colleagues evaluated NENU-3 (HKUST-1 loaded with phosphotungstic acid) as a proton-conducting material.[55] The introduction of $H_3PW_{12}O_{40}$ improved the retention of water molecules in the pores of HKUST-1, even at 90 °C. Consequently, proton transfer was facilitated, and the activation energy was reduced to 0.41 eV in NENU-3 (*vs.* 0.69 eV in HKUST-1), and conductivity increased to 4.76×10^{-5} S cm^{-1} at 90 °C under 70% RH (refer to the fact that the conductivity of pristine HKUST-1 was 1.08×10^{-8} S cm^{-1} under same conditions). Inspired by these results, authors sought to further improve the conductivity of NENU-3 by exchanging Cu-coordinated water molecules with isonicotinic acid (Ina), which could act both as a proton donor and H-bonding acceptor, as pictured in Fig. 3(c).

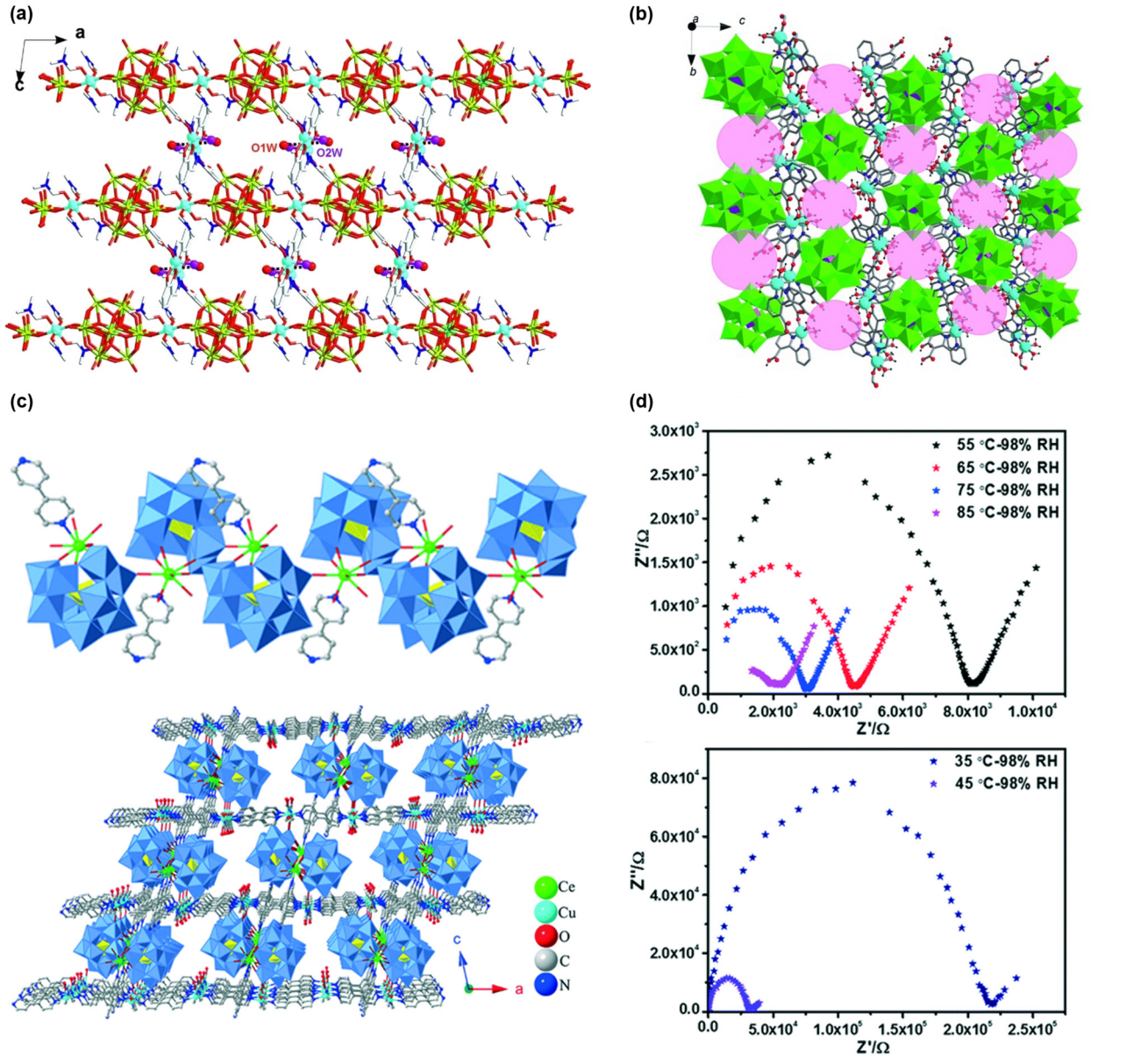

Fig. 2 (a) View of the 2D organic–inorganic composite layer with hydrophilic cavities from the "ABAB" packing arrangement of the metal-Schiff-base cations and 1D organic–inorganic anionic chains along the *ac* plane. Cu, O, Si, N and W are represented as cyanine, red, green, blue and yellow, respectively. Reproduced with permission from ref. 49, Copyright 2014, Wiley, VCH. (b) View of the 3D $[\{Cu(Hbpdc)(H_2O)_2\}_2\{PM_{12}O_{40}\}]^{n-}$ unit with 1D the hydrophilic channels (pink circles) along the *a* axis. Reproduced with permission from ref. 51, Copyright 2013, Wiley, VCH. (c) The structure of the 1D chain in **1**; and the view of the 3D framework structure in **1**. Polyhedral codes: WO_6, blue; PO_4, yellow. (d) Nyquist plots for **1** at different temperatures at 98% RH; reproduced with permission from ref. 52, Copyright 2021, Royal Society of Chemistry.

Proton conductivity in NENU-3-Ina reached 1.81×10^{-3} S cm^{-1} at 90 °C under 70% RH, and its E_a was 0.36 eV. Later, when instead of Ina, imidazole (Im) was loaded in NENU-3 to give Im@NENU-3, conductivity improved by an order of magnitude 1.82×10^{-2} S cm^{-1} at 90 °C under 70% RH, which could be maintained up to 12 h, as investigated by Ye and coauthors.[56] Notably, they found that the strategy followed for loading the Im had a huge effect on the conductivity of the resulting material, as schematized in Fig. 3(d). When Im was loaded in a pristine NENU-3, with water molecules coordinated to the Cu center to obtain Im@NENU-3, it resulted in a high concentration of free imidazole molecules in the pores. Thus, the proton conductivity was two orders of magnitude higher than that of Im-loaded activated NENU-3 (Im-Cu@NENU-3a), where Im was coordinated to Cu centers and in a lesser amount than Im@NENU-3. This result manifested that forming an extended H-bond network (promoted by a high concentration of free imidazole and water molecules, as illustrated in Fig. 3(e)–(j)) was indispensable to reach good proton conductivities. Although the conductivity of Im@NENU-3 was higher than that of previously reported NENU-3-Ina, the activation energy of Im@NENU-3 was slightly higher (0.57 eV).

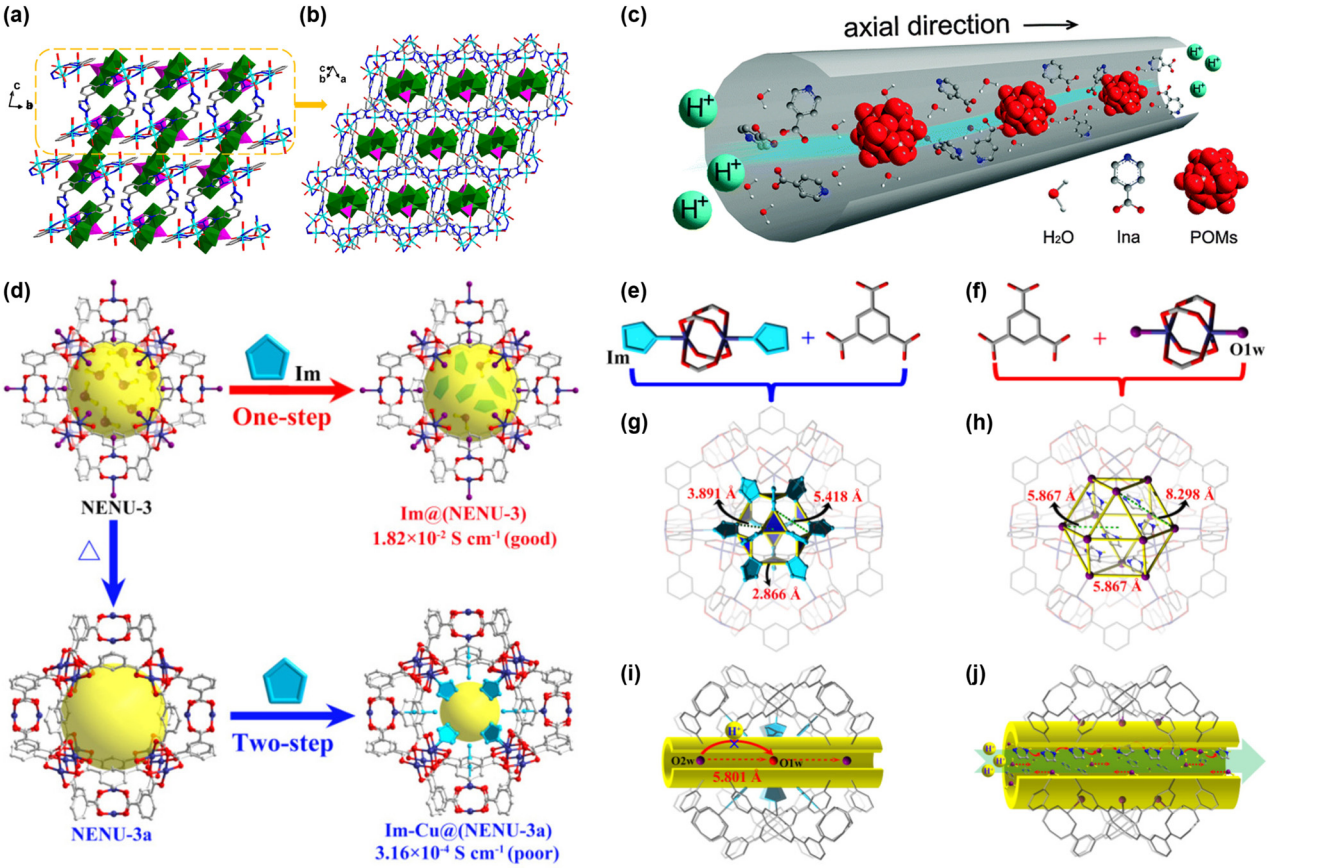

Fig. 3 Summary of the structure of **NENU-530**: (a) ball-and-stick representation of the packing arrangement of staggered 2D sheet-like structure in **NENU-530**. (b) The 3D framework of **NENU-530**. Reproduced with permission from ref. 54, Copyright 2016, Wiley, VCH. (c) Schematic of the proton-conducting pathway constructed by POMs, Ina and water molecules arranged alternately in the nano-channels. Reproduced with permission from ref. 55, Copyright 2014, Royal Society of Chemistry. (d) Comparison of the one- and two-step synthesis of the proton conductors **Im@(NENU-3)** and **Im-Cu@(NENU-3a)**, and their corresponding proton conductivities. BTC ligand and the paddle-wheel Cu_2 units in **Im-Cu@(NENU-3b)** (e) and **NENU-3** (f). The cuboctahedral cage B in **Im-Cu@(NENU-3b)** (g) and **NENU-3** (h) are fabricated by the BTC ligands and the Cu_2 units, and with the different pore spaces and window sizes with much more free imidazole molecules inside the pore spaces of **NENU-3**. (i) Speculative pathway of the proton conduction for **Im-Cu@(NENU-3a)** based on single crystal X-ray data showing the actual positions of the absorbed water molecules within the structure. (j) Schematic view of the possible proton-conductive pathways in **Im@(NENU-3)**. Water molecules are shown in violet or red. Red arc arrows show the protons hop along hydrogen-bonding networks. Red dashed arrows represent transport of protons through self-diffusion of protonated water. (Guest molecules and H atoms are omitted for clarity.) Reproduced with permission from ref. 56, Copyright 2017, American Chemical Society.

The inclusion of POMs in Cu-MOFs has resulted in moderate enhancement of proton conductivity, as summarized in Table 1. No significant differences in structure and proton-conducting properties were observed between these compounds, implying that metal in the POM is irrelevant to its proton-conduction pathway. However, its moisture retention ability is enhanced by its high hydrophilicity and water capture ability, and it conducts enhanced proton conductivity in relatively low humid conditions and high temperatures. Notably, both compounds retained water molecules up to 100 °C;

Table 1 Summary of proton-conductivities of Cu-MOFs incorporating POMs

Material	σ (S cm^{-1})	E_a (eV)	Temperature (°C)	% RH	Ref.
$[\{Cu_3(L)_2(H_2O)_4\}\{Cu(dmf)_4(SiW_{12}O_{40})\}\cdot 9H_2O]_n$[a]	5.94×10^{-4}	0.32	100	98	49
$Cu_3Mo_5P_2$	2.2×10^{-5}	0.23	28	98	50
$[H\{Cu(Hbpdc)(H_2O)_2\}_2(PMo_{12}O_{40})\cdot nH_2O]_n$	1.25×10^{-3}	1.02	100	98	51
$[H\{Cu(Hbpdc)(H_2O)_2\}_2(PW_{12}O_{40})\cdot nH_2O]_n$	1.56×10^{-3}	1.02	100	98	51
$[\{Cu_4(dpdo)_{12}\}\{H(H_2O)_{27}(CH_3CN)_{12}\}(PW_{12}O_{40})_3]_n$	1.25×10^{-4}	0.82	100	98	53
NENU-3	4.76×10^{-5}	0.41	90	70	55
NENU-3-Ina	1.81×10^{-3}	0.36	90	70	55
HKUST-1	1.08×10^{-8}	0.69	90	70	55
Im@NENU-3	1.82×10^{-2}	0.57	90	70	56

[a] L = *N*,*N*′-bis[(2-hydroxy-3-methoxyphenyl)methylidene]hydrazine hydrate.

however, activation energy was exceptionally high (1.02 eV) among the POM-Cu-MOFs reviewed. The insertion of POMs in $Cu_3(BTC)_2$ (BTC = benzentricarboxylate; also referred to as HKUST-1) to produce NENU-3 improved its proton conductivity; however, the best values were obtained for NENU-3 loaded with additional H-bond-forming entities like isonicotinic acid (Ina) or proton carriers like imidazole (Im). Of the eight materials, only Im@NENU-3 was evaluated for long-term proton conductivity (12 hours), successfully demonstrating its structural stability by using PXRD measurements.

2.2. Incorporating protic guest molecules

Encapsulation of guest molecules was one of the strategies explored to study and enhance proton conductivity in MOFs. Our group reported a conceptual example that proton conductivity could be tuned by changing the coordinating solvent molecules at Cu(II) centers in HKUST-1.[57] While protic solvent molecules residing in the pores of HKUST-1 typically form a simple H-bond network without proton conduction, coordinating water molecules at Cu centers trigger forming the H-bond network to transfer protons and thereby transform it into a conductive one. Although water is generally a poor proton donor, its acidity increases when coordinated to a transition metal center, enabling it to donate protons to pore-filling protic solvent molecules such as methanol (MeOH), as shown in Fig. 4(a) and (b). Consequently, the conductivity of H_2O-loaded HKUST-1 (H_2O-HK) reached 1.5×10^{-5} S cm^{-1} at room temperature under a MeOH atmosphere. Moreover, the acidity of the coordinated molecules plays a decisive role in proton conduction: low-acidic solvent molecules (MeOH or EtOH) do not provide sufficient protons to impact conductivity significantly (Fig. 4(c)).

Building on this concept, Khatua and coworkers explored the effect of various guest molecules in the pores of MOFs. They employed a Cu(I)-MOF with a V-shaped flexible terpyridine-based linker $[\{(C_{44}H_{48}O_9Cu_2I_2)_n\}\supset(DMF)(MeCN)]$ and loaded different molecules such as H_2O, MeOH, dimethyl sulfoxide (DMSO), *N*,*N*′-dimethylformamide (DMF), diethylamine (DEA), nitrobenzene (NB), 1,4-dinitrobenzene (DNB), pyridine (py), and 1*H*-1,2,4-triazole (tz).[58] Under anhydrous conditions, the conductivity was negligible without guest molecules. However, conductivity improved significantly under humid conditions (95% RH), exceeding 10^{-3} S cm^{-1} for several combinations, including $[\{(C_{44}H_{48}O_9Cu_2I_2)_n\}\supset\mu(H_2O)(DMF)]$, $[\{(C_{44}H_{48}O_9Cu_2I_2)_n\}\supset NB]$, $[\{(C_{44}H_{48}O_9Cu_2I_2)_n\}\supset DNB]$, $[\{(C_{44}H_{48}O_9Cu_2I_2)_n\}\supset py]$, and $[\{(C_{44}H_{48}O_9Cu_2I_2)_n\}\supset tz]$. The highest values were observed for $[\{(C_{44}H_{48}O_9Cu_2I_2)_n\}\supset(H_2O)(DMF)]$ (1.89×10^{-3} S cm^{-1} at 65 °C) and $[\{(C_{44}H_{48}O_9Cu_2I_2)_n\}\supset tz]$ (2.89×10^{-3} S cm^{-1} at 80 °C) (Fig. 4(d)).

The correlation between proton conductivity and the species of solvent molecules highlights the importance of H-bonds, particularly involving water molecules, in achieving high conductivity. Zhang and colleagues proposed that a MOF with linkers containing a high proportion of oxygen (O) and nitrogen (N) atoms could retain adsorbed water molecules even at reduced RH, thereby maintaining good conductivity.[59] The authors prepared an ionic Cu-based MOF using 4-carboxypyrazole (Cpz) as a linker,

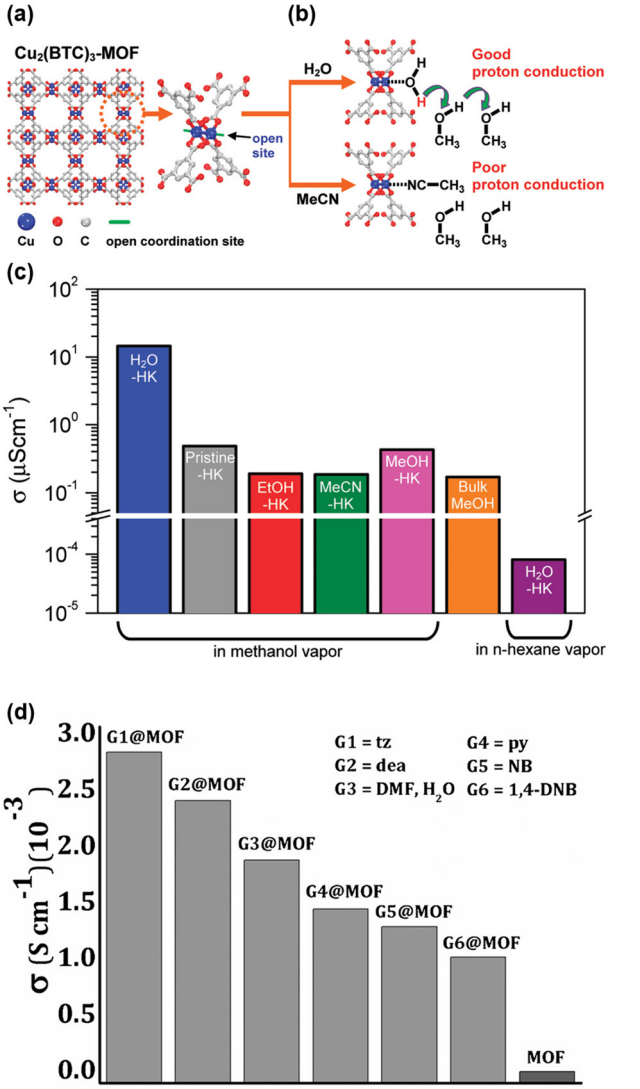

Fig. 4 (a) Illustrations of the HKUST-1 structure in a two-dimensional view along the (100) direction. (b) HKUST-1 nodes with the Cu-paddlewheel environment and qualitative representations of proton transfer from Cu(II) centers coordinated with water and ethanol. (c) Proton conductivities of H_2O-HK, pristine-HK, EtOH-HK, MeCN-HK, MeOH-HK, and bulk MeOH under a MeOH or *n*-hexane atmosphere as indicated. Reproduced with permission from ref. 57, Copyright 2012, American Chemical Society. (d) Bar diagram representation of the proton conductivities of the activated complex [**1**] and its guest-incorporated adducts. Reproduced with permission from ref. 58, Copyright 2016, Wiley, VCH.

specifically $NH_4[Cu_3(OH)(C_4H_2N_2O_2)_3]$ (hereafter CuCpz), an anionic framework built from $Cu_3(\mu_3\text{-OH})$ bridges connected by Cpz linkers (Fig. 5(a)–(c)). This framework could absorb up to 385 water molecules per unit cell at 25 °C due to the presence of hydrophilic atoms (Cu(II), O, and N) and counter cations (NH_4^+). Remarkably, during desorption, water contents remained at 385 water molecules per unit cell until the relative humidity dropped to 40%. The conductivity of CuCpz reached 2.45×10^{-3} S cm^{-1} at 100% RH, and it only decreased to 1.26×10^{-3} S cm^{-1} when RH was lowered to 43%. Notably, to achieve 1.26×10^{-3} S cm^{-1} at 43% RH, CuCpz needed to be saturated with water before

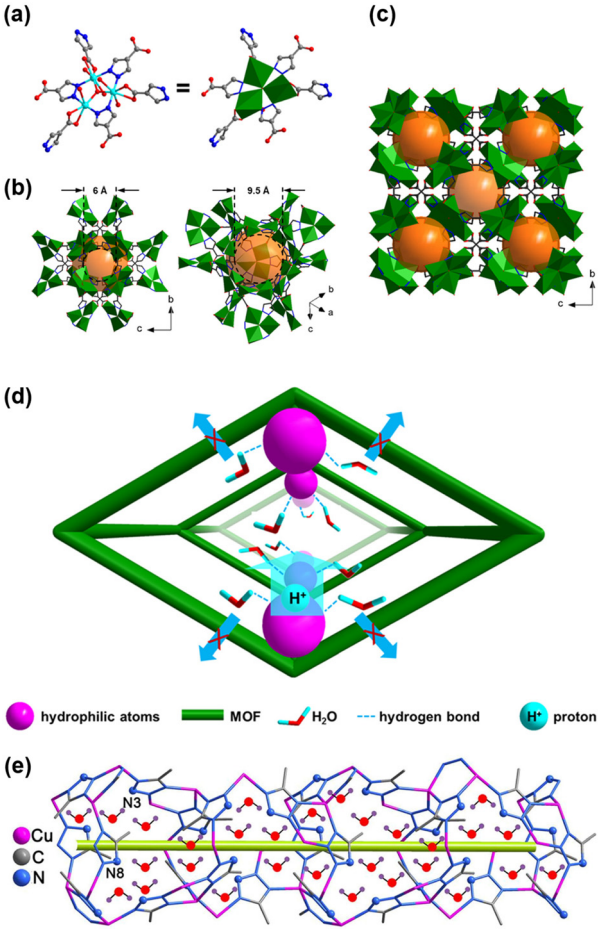

Fig. 5 Schematic diagrams of CuCpz. (a) $Cu_3(\mu_3\text{-}OH)$ clusters in CuCpz; (b) accessible window apertures of the cage structure; and (c) unit cell. All NH_4^+ ions in the pore and the hydrogen atoms of the ligands are omitted for clarification. The Cu, O, N, and C are shown in cyan, red, blue, and gray, respectively. (d) Proposed holding effect scheme of the hydrophilic atoms in the CuCPz pores for enhancing the proton conductivity at reduced RH. Reproduced with permission from ref. 59, Copyright 2022, American Chemical Society. (e) Tunnel in the 3D anionic $[Cu_3(mtz)_4]^-$ framework of 1 with schematic guest water molecules. Red and purple balls present O and H atoms, respectively. The green, yellow bar highlights the proton pathway. Reproduced with permission from ref. 64, Copyright 2021, American Chemical Society.

reducing the RH. When the RH was directly set to 40% from a dry state, conductivity was significantly lower at only 1×10^{-6} S cm^{-1}, indicating that the abundance of hydrophilic atoms created a robust H-bond network that helped retain water molecules as humidity levels decreased (Fig. 5(d)).

Due to the small size of guest molecules relative to the large pore space, substantial disorder among the filling molecules was observed, making it challenging to establish clear correlations between conductivity and interactions among guest molecules, the host framework, and proton carriers. To improve the molecular ordering within the framework, the addition of functional groups to the linker that can form strong H-bonds with water molecules in the pores is a viable approach. For example, Gil-Hernández and colleagues utilized a mesoxalate linker to build two anionic Cu-MOFs $[(H_3O)\{Cu_7(Hmesox)_5(H_2O)_7\}\cdot 9H_2O]_n$ and $[(NH_4)_{0.6}(H_3O)_{0.4}\{Cu_7(Hmesox)_5(H_2O)_7\}\cdot 11H_2O]_n$ (mesox = mesoxalate), which contains carboxylate and hydroxyl groups to stabilize water molecules.[60] In these frameworks, conductivity arose from cations (H_3O^+ and NH_4^+) located in the pore space alongside crystallized water molecules. Despite the presence of different cations, the conductivity did not significantly differ between these materials: both showed nearly identical proton conduction behavior, reaching maximum conductivity at 23 °C under 100% RH (6.5×10^{-5} S cm^{-1}) and decreasing by three orders of magnitude after heating to 85 °C, in which conditions water loss occurred, disrupting the H-bond network.

In a subsequent study, Gil-Hernández and coworkers investigated the impact of different cations on the proton-conducting properties of three new mesoxalate-based Cu-MOFs: $(H_3O)[Cu_9(Hmesox)_6(H_2O)_6Cl]\cdot 8H_2O$, $(NH_2Me_2)_{0.4}(H_3O)_{0.6}[Cu_9(Hmesox)_6(H_2O)_6Cl]\cdot 8H_2O$, and $(enH_2)_{0.25}(enH)_{1.5}[Cu_6(Hmesox)_3(mesox)(H_2O)_6Cl_{0.5}]Cl_{0.5}\cdot 5.25H_2O$ (NH_2Me_2 = dimethylammonium, enH_2, enH = ethylenediammonium).[61] Unlike their previously reported materials, the conductivity of all three new MOFs increased as the temperature increased up to 80 °C, showing the highest conductivity (1.87×10^{-3} S cm^{-1}) at 80 °C under 95% RH for $(enH_2)_{0.25}(enH)_{1.5}[Cu_6(Hmesox)_3(mesox)(H_2O)_6Cl_{0.5}]Cl_{0.5}\cdot 5.25H_2O$. This improvement in conductivity was attributed to three main factors: (1) a greater number of coordinated water molecules compared to the other two compounds; (2) stronger interactions between crystallized water molecules and the framework, which assists in retaining water molecules at higher temperatures; and (3) in $(enH_2)_{0.25}(enH)_{1.5}[Cu_6(Hmesox)_3(mesox)(H_2O)_6Cl_{0.5}]Cl_{0.5}\cdot 5.25H_2O$, the mesoxalate was fully deprotonated, supplying an extra proton carrier to maintain charge neutrality and thereby, resulting in proton carriers three times more than in $(H_3O)[Cu_9(Hmesox)_6(H_2O)_6Cl]\cdot 8H_2O$ and $(NH_2Me_2)_{0.4}(H_3O)_{0.6}[Cu_9(Hmesox)_6(H_2O)_6Cl]\cdot 8H_2O$. These findings highlight the importance of both the number and nature of proton carriers in determining conductivity.

Improving the concentration and ordering proton carriers further enhances conductivity.[66,67] One effective approach involves incorporating biomolecules, such as amino acids, peptides, or polysaccharides, into MOFs. Grancha and coworkers reported an MOF, $[Ca(II)Cu(II)_6\{(S,S)\text{-alamox}\}_3(OH)_2(H_2O)]\cdot 32H_2O$, using an oxamidato linker {(*S*,*S*)-alamox} driven from natural amino acids.[62] This material featured honeycomb-like hexagonal channels filled with H-bonded water molecules forming a 1D ribbon array. The highly ordered water molecules enabled modest conductivity (8.6×10^{-4} S cm^{-1} at 80 °C under 95% RH). Based on the crystal structure and theoretical calculations, the authors proposed a Grotthuss-type proton-hopping mechanism involving the cleavage and formation of covalent O–H bonds, followed by a reorganization of solvent molecules within the pores.

Another example comes from Li and colleagues, who synthesized a 2D homochiral MOF based on L-hydroxyproline: $[Cu_2(Htzehp)_2(4,4'\text{-bipy})]\cdot 3H_2O$ (Htzehp = *N*-[2-(1*H*-tetrazol-5-yl) ethyl]-L-hydroxyproline).[63] This MOF achieved anisotropic conductivity of 1.39×10^{-4} S cm^{-1} at 30 °C under 95% RH along the [100] direction, compared to the conductivity two orders of magnitude lower in the [010] direction under the same

Table 2 Summary of proton-conductivities of Cu-MOFs incorporating H-bonded guest molecules or functionalities

Material	σ (S cm^{-1})	E_a (eV)	Temperature (°C)	% RH	Ref.
H_2O-HK	1.5×10^{-5}	NR	25	—	57
MeCN-HK	2.0×10^{-7}	NR	25	—	57
EtOH-HK	2.0×10^{-7}	NR	25	—	57
$[\{(C_{44}H_{48}O_9Cu_2I_2)_n\} \supset$ deal]	3.77×10^{-7}	0.79	50	0	58
$[\{(C_{44}H_{48}O_9Cu_2I_2)_n\} \supset (H_2O)(DMF)]$	1.89×10^{-3}	1.10	65	95	58
$[\{(C_{44}H_{48}O_9Cu_2I_2)_n\} \supset$ tz]	2.89×10^{-3}	1.55	80	95	58
CuCpz	1.80×10^{-2}	0.33	80	100	59
$[(NH_4)_{0.6}(H_3O)_{0.4}\{Cu_7(Hmesox)_5(H_2O)_7\}\cdot 11H_2O]_n$	6.5×10^{-5}	NR	23	100	60
$[(H_3O)\{Cu_7(Hmesox)_5(H_2O)_7\}\cdot 9H_2O]_n$	6.5×10^{-5}	NR	23	100	60
$(H_3O)[Cu_9(Hmesox)_6(H_2O)_6Cl]\cdot 8H_2O$	1.16×10^{-4}	0.43 to 0.5	80	95	61
$(NH_2Me_2)_{0.4}(H_3O)_{0.6}[Cu_9(Hmesox)_6(H_2O)_6Cl]\cdot 8H_2O$	1.85×10^{-4}	0.43 to 0.5	80	95	61
$(enH_2)_{0.25}(enH)_{1.5}[Cu_6(Hmesox)_3(mesox)(H_2O)_6Cl_{0.5}]Cl_{0.5}\cdot 5.25H_2O$	1.87×10^{-3}	0.43 to 0.5	80	95	61
$[Ca^{II}Cu^{II}_6\{(S,S)$-alamox$\}_3(OH)_2(H_2O)]\cdot 32H_2O$	8.6×10^{-4}	0.34	80	95	62
$[Cu_2(Htzehp)_2(4,4'$-bipy$)]\cdot 3H_2O$	1.39×10^{-4}	0.48	30	95	63
$NaCu_3(mtz)_4$	1.33×10^{-2}	0.34	70	100	64
NH_4Br@HKUST-1	8.99×10^{-4}	0.68	25	99	65
HKUST-1	1.04×10^{-8}	1.42	25	99	65

conditions. Activation energies along the [100] and [010] directions were 0.48 eV and 0.56 eV, respectively, suggesting different proton transport mechanisms: a Grotthuss-type mechanism in the [100] direction, while a vehicle mechanism in the [010] direction.

Tetrazoles, known for forming H-bonds due to their nitrogen-rich structure, also demonstrate potential as MOF linkers. Lu and colleagues synthesized an ultra-stable $NaCu_3(mtz)_4$ (mtz = 5-methyltetrazolate), which exhibited good thermal and chemical stability.[64] The material demonstrated outstanding proton conductivity (1.33×10^{-2} S cm^{-1}) at 70 °C under 100% RH, with an E_a of 0.34 eV, indicative of Grotthuss-type proton conduction (Fig. 5(e)).

Introducing ion pairs within MOF cavities to form clathrates has also proven effective. You and coauthors demonstrated the enhanced proton conductivity of benchmark HKUST-1 by incorporating NH_4Br (NH_4Br@HKUST-1).[65] Proton conductivity significantly increased under high relative humidity (99% RH) up to 8.99×10^{-4} S cm^{-1}, while pristine HKUST-1 alone remained low in conductivity (10^{-8} S cm^{-1}). Though NH_4Br@HKUST-1 displayed a higher activation energy than HKUST-1 (1.42 eV *vs.* 0.69 eV), the primary transport mechanism remained the vehicle type in both materials. These results demonstrate that the insertion of additional guest molecules capable of improving proton transport pathways can yield high conductivity ($\sim 10^{-3}$ S cm^{-1}) in some cases, as seen in $[\{(C_{44}H_{48}O_9Cu_2I_2)_n\} \supset (H_2O)(DMF)]$ and $[\{(C_{44}H_{48}O_9Cu_2I_2)_n\} \supset$ tz] (Table 2).

2.3. Ligand functionalization

Developing proton-conducting materials that perform well under low humidity conditions is essential to ensure reliable PEM performance across diverse applications. This aim can be achieved by creating H-bonds pathways using fewer guest molecules through ligand functionalization. This section discusses two primary strategies: exploiting ligands with (1) H-bonding capabilities and (2) highly acidic properties.

The first strategy, which uses H-bond-forming ligands, typically employs pyridine or pyrazole-based ligands that contain nitrogen atoms for forming H-bonding. Ruan and coauthors reported $[Cu(atz)_2(H_2O)_2]\cdot H_2O$ (Hatz = 5-aminotetrazole) MOFs, where the atz ligand forms a two-dimensional framework by connecting two Cu(II) ions (Fig. 6(a)).[68] The atz ligand can act as both a proton donor and acceptor, allowing water molecules to create H-bond pathways that serve as proton conduction channels (Fig. 6(b)). Similarly, Tayade and colleagues designed MOFs with bipyridine glycoluril, with N–H bonds acting as H-bond donors and C=O bonds acting as H-bond acceptors.[69] This MOF forms H-bonds when water molecules coordinate with the MOF, creating aligned H-bond networks that act as proton conduction pathways (Fig. 6(c)).

Multifunctional organic linkers, where highly electronegative atoms such as nitrogen, oxygen, or sulfur are rich, can provide a suitable pore environment for good proton transport. For example, Li's group developed a 2D layered Cu-MOF, $[Cu(p\text{-IPhHIDC})]_n$, using an imidazole-based linker (p-IPhH_3IDC = 2-(p-*N*-imidazol-1-yl)phenyl-1*H*-imidazole-4,5-dicarboxylic acid).[70] Notably, some carboxylic acid groups protonated within the framework resulted in a proton conductivity of 1.51×10^{-3} S cm^{-1} at 100 °C under 98% RH due to H-bond networks with interlayer water molecules. In contrast, a similar Cu-MOF ($[Cu_4(HDMPhIDC)_4(H_2O)_4]_n$), where H_3DMPhIDC is 2-(3,4-dimethyl)phenyl-4,5-imidazole dicarboxylic acid, showed a conductivity of 2.58×10^{-5} S cm^{-1} at the same temperature and humidity.[71] Although both $[Cu(p\text{-IPhHIDC})]_n$ and $[Cu_4(HDMPhIDC)_4(H_2O)_4]_n$ contained uncoordinated carboxylic acid groups, the higher nitrogen content in $[Cu(p\text{-IPhHIDC})]_n$ provided more proton hopping sites for higher proton conductivity. This result suggests that the number of N-atoms plays a crucial role in conductivity, even though differences in the overall structure are not considered.

Continuing with this approach, Li's group further studied a thiourea-based metal-mixed Cu(I/II)-MOF, featuring a complex H-bond system formed by interactions among O-, N-atoms from the linker, free water, methanol, and coordinated DMF molecules: $[\{Cu(I)_3Cu(II)_3L_3(DMF)_2(CH_3OH)(H_2O)\}\cdot 3CH_3OH]_n$, where L represents [3-(4-methyl-benzoyl)-thioureido]-acetic acid.[72] This MOF, noted for its high thermal and chemical

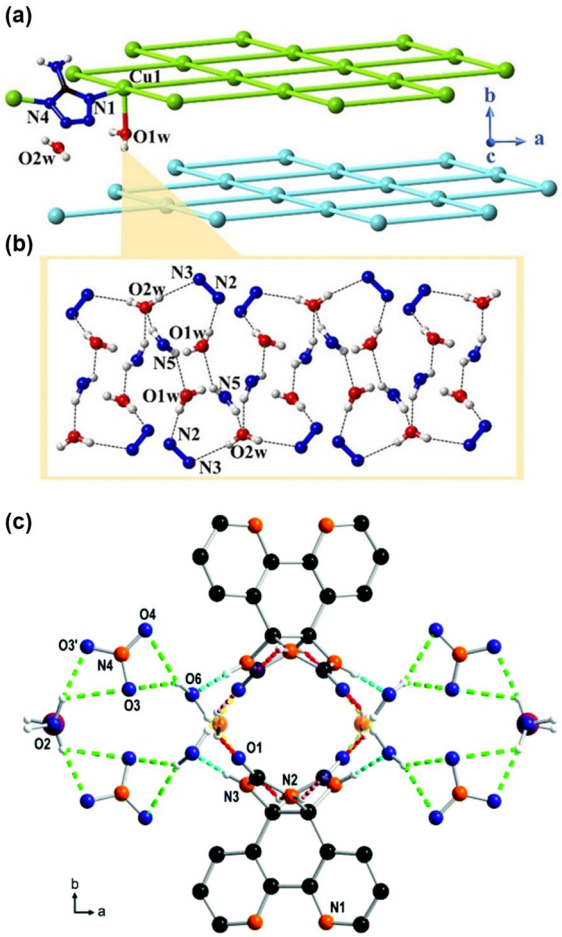

Fig. 6 (a) The stacking **sql** networks for complex **1**, among that atz^- ligands can be considered as sticks. (b) The coordinated water molecules O1w and free water molecules O2w are linked into 1D hydrogen transport channel by hydrogen bonds with atz^- ligands. Reproduced with permission from ref. 68, Copyright 2021, Wiley, VCH. (c) Ligand NH···O (red) ligand donor–acceptor bonds are responsible for the formation of channels along [001]. In addition ligand NH···O water (bluish), water OH···O nitrate (green) and water OH···O ligand (yellow) hydrogen donor–acceptor bonds are observed (color code: N = orange, O = blue and Cu = purple). Reproduced with permission from ref. 69, Copyright 2017, Royal Society of Chemistry.

stability, exhibited a conductivity of 3.78×10^{-4} S cm^{-1} at 98% RH and 100 °C, which was one order of magnitude higher than the conductivity of the H-bonded organic framework formed solely by the linker, L. The improved conductivity was attributed to higher proton mobility facilitated by free solvent molecules, particularly water, within the channels of the Cu(I/II)-MOF.

The second strategy involves incorporating highly acidic functional groups, like sulfonic acid, into MOFs. Organic polymers containing sulfonic acid, such as Nafion, are known for their high proton conductivities ($\sim 10^{-1}$ S cm^{-1}) due to the strong Brønsted acidity of sulfonic acids and their ability to form extended H-bond networks.[73–75] Inspired by such polymers, Cu-MOFs with sulfonic acid or sulfonate groups on their framework linkers have been extensively studied. For instance, disodium-2,2′-disulfonate-4,4″-oxydibenzoic acid (Na_2H_2DSOA) formed a porous 3-dimensional MOF, Cu-DSOA, based on a tetrameric copper-cluster framework with H_3O^+ ions as charge-balancing cations (Fig. 7(a) and (b)).[76] Proton conductivity was relatively low (10^{-6} S cm^{-1}) at room temperature, even under high relative humidity (98% RH), but increased significantly, reaching 1.9×10^{-3} S cm^{-1} at 85 °C under the same humidity. The relatively high activation energy (1.04 eV) indicates that proton transfer likely occurs through the vehicle mechanism, suggesting that the long-range directional mobility of H_3O^+ ions improves as the temperature increases, and this behavior, along with the higher dielectric constant of water molecules at elevated temperatures, contributes to enhanced conductivity. Another example is $Cu_4(L)_2(OH)_2(DMF)_2$, where L represents 5-sulfoisophthalate.[38] This MOF features a tetranuclear Cu cluster and irregular 1D channels lined with abundant H-bonds between sulfonate/carboxylate groups and DMF molecules (Fig. 7(c)–(f)).[77] The highest conductivity recorded in this MOF was 7.4×10^{-4} S cm^{-1} at 95 °C under 95% RH.

Combining these two strategies by mixing different ligands—one containing H-bond-forming groups (like pyridine, pyrazole, or

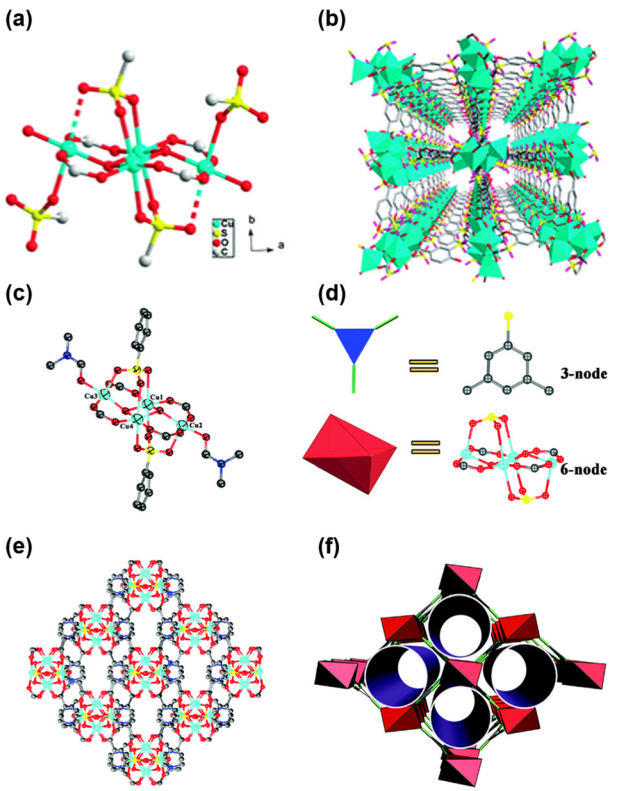

Fig. 7 (a) A view of a tetrameric copper cluster. (b) Central projection of Cu-DSOA viewed down the *c*-axis. The solvent water molecules and hydrogen atoms are omitted for clarity. Reproduced with permission from ref. 76, Copyright 2013, Royal Society of Chemistry. (c) The asymmetric unit of **1**; (d) the three-dimensional structure viewed along the *b*-axis; (e) ball-and-stick and polyhedral representations of the 3-connected L ligand and 6-connected $[Cu_4(OH)_2(CO_2)_4(SO_3)_2]$ cluster, respectively; (f) the (3,6)-connected 3D non-interpenetrating network of **1**. Reproduced with permission from ref. 77, Copyright 2015, Royal Society of Chemistry.

amine) and the other containing sulfonate groups—can also improve conductivity. For instance, the mixed-linker Cu-MOF $[\{Cu_2(sba)_2(bpg)_2(H_2O)_3\}\cdot 5H_2O]_n$, where sba is 4-sulfobenzoate, and bpg is bipyridine glycoluril, exhibited one-dimensional chains of water molecules filled in hydrophilic channels (Fig. 8(a)).[78] The maximum conductivity, 0.94×10^{-2} S cm^{-1} at 80 °C under 95% RH, was attributed to the presence of extensive networks of H-bonded water molecules interacting with the uncoordinated oxygens of sulfonate, carboxylate, and glycoluril groups in the wall of MOF channels.

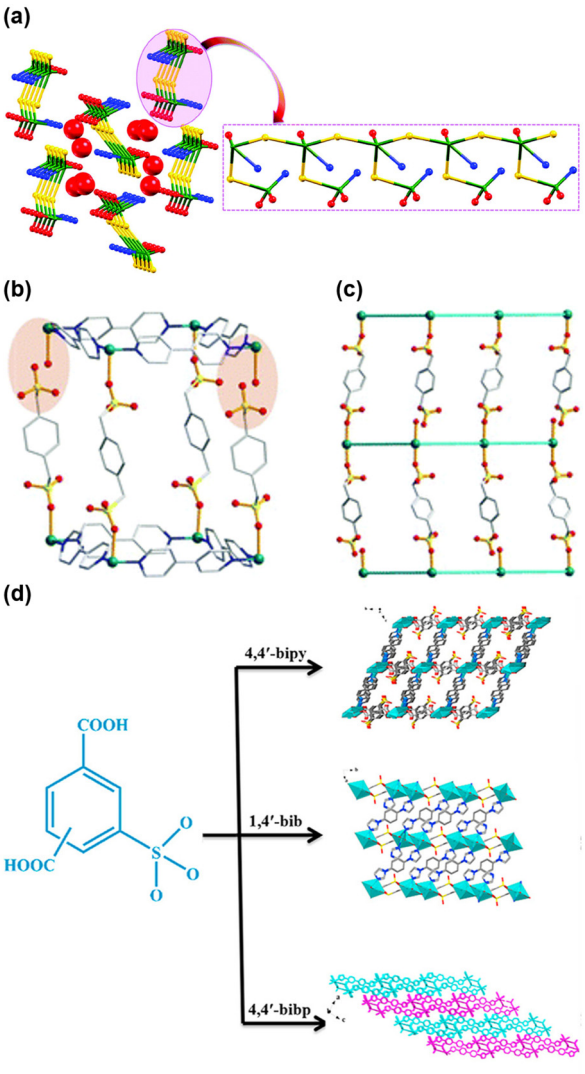

Fig. 8 (a) Showing the node-and-linker-type representation of 1D chain in **1**; the copper nodes are represented in green, sba linkers in yellow, BPG ligands in blue and water molecules are in red colour. Reproduced with permission from ref. 78, Copyright 2019, Royal Society of Chemistry. Crystallographic view of TMOF-2 (Cu, teal; C, gray; S, yellow; O, red; N, blue): (b) one single primitive-cubic net with the missing metal–ligand connectivities highlighted; (c) a single primitive extended framework viewed along the a axis in which 4,4′-bipy is simplified as a rod for clarity; reproduced with permission from ref. 79, Copyright 2017, Royal Society of Chemistry. (d) Three new Cu(II) coordination polymers, $[Cu_5(\mu_3\text{-}OH)_4(STP)_2(4,4'\text{-}bipy)_2(H_2O)_2]\cdot 4H_2O$ (CTGU-20), $[Cu_2(\mu_2\text{-}OH)(SIP)(1,4'\text{-}bib)_2]$ (CTGU-21) and $[Cu_2(SIP)(4,4'\text{-}bibp)_2(HCOO)]\cdot 3H_2O$ (CTGU-22) and based on two less-developed isomeric sulfo-functionalized benzene dicarboxylic acid linkers were synthesized and characterized. Reproduced with permission from ref. 80, Copyright 2021, Elsevier.

Although organosulfonates are known to create relatively fragile frameworks due to their weak coordination with metal cations, the incorporation of sulfonate groups into MOFs has been explored to improve conductivity. Notably, Zhang and coauthors reported the doubly interpenetrated and permanently porous TMOF-2, constructed using copper nitrate, 1,4-benzenedimethanesulfonate (1,4-BDMS), and 4,4′-bipyridine (4,4′-bipy).[79] The TMOF-2 structure showed dangling sulfonate groups and open Cu(II) sites, forming a network of H-bonded water molecules upon adsorption and thereby creating effective pathways for proton transport (Fig. 8(b) and (c)). As a result, TMOF-2 achieved a conductivity of 1.23×10^{-4} S cm^{-1} with an E_a of 0.37 eV, consistent with a proton-hopping (Grotthuss) mechanism.

Moi and coauthors further explored using a mixture of two different ligands: 1,2,4-triazol-4-amine (T4A) as an H-bond-forming component and 1,5-naphthalenedisulfonic acid as an acidic group. Incorporating amine and sulfonates into a MOF created an appropriate distance between these functional groups, resulting in a high proton conductivity of 0.53×10^{-3} S cm^{-1} at 80 °C and 98% RH.[81] Additionally, a number of oxygen atoms from sulfonate groups available to form H-bonds and guest water molecules influenced conductivity, as exemplified by Cu-MOFs such as CTGU-20, CTGU-21, and CTGU-22, reported by Yu and colleagues.[80] While all three frameworks are of difference in structure as depicted in Fig. 8(d), CTGU-20 displayed the highest conductivity (2.86×10^{-4} S cm^{-1} under 98% RH), seemingly due to its completely uncoordinated sulfonate groups, which were closely spaced and allowed efficient water molecule retention.

Phosphonates have also been studied for their potential as building blocks for proton-conducting MOFs due to their uncoordinated acidic hydroxyl groups, which can form H-bond networks with guest water molecules. For instance, BAM-3, $[Cu(H_2PhDPA)(dpe)_2(H_2O)_2\cdot 2H_2O]_n$ (with H_2PhDPA = phenylene diphosphonate and dpe = 1,2-di(4-pyridyl)ethylene), reported by Rautenberg and coworkers in 2022, demonstrated modest conductivity of 1.4×10^{-5} S cm^{-1} at 50 °C under 98% RH, although it was suffered from dehydration and a phase transition above 50 °C, which negatively affected its performance.[82]

CuCpz and $NaCu_3(mtz)_4$, anionic MOFs based on N-rich linkers (Cpz = 4-carboxypyrazole and mtz = 5-methyltetrazolate, respectively) exhibited the best proton conductivities ($>10^{-2}$ S cm^{-1}). CuCpz, which displayed the highest conductivity at 80 °C under 100% RH among the materials discussed in this section, maintained conductivity for up to 120 hours without notable structural damage, even as relative humidity was lowered from 100% RH to 43% RH. This stability contrasts with many other materials, which typically experience an abrupt decrease in conductivity when humidity levels drop. In the case of $NaCu_3(mtz)_4$, its proton conductivity was elevated and remained stable for up to 8 hours, although it required high humidity to achieve these results. Despite numerous uncoordinated nitrogen atoms available to

Table 3 Summary of proton-conductivities of Cu-MOFs incorporating sulfonic or sulfonate groups

Material	σ (S cm^{-1})	E_a (eV)	Temperature (°C)	% RH	Ref.
Cu-DSOA	1.9×10^{-3}	1.04	85	98	76
$Cu_4(L)_2(OH)_2(DMF)_2$[a]	7.4×10^{-4}	1.32	95	95	77
$[\{Cu_2(sba)_2(bpg)_2(H_2O)_3\}\cdot 5H_2O]_n$	0.94×10^{-2}	0.64	80	95	78
TMOF-2	1.23×10^{-4}	0.37	90	98	79
CTGU-20	2.86×10^{-4}	NR	50	98	80
CTGU-21	1.58×10^{-5}	NR	50	98	80
CTGU-22	4.58×10^{-5}	NR	50	98	80

[a] L = 5-sulfoisophthalate.

form H-bonds and facilitate efficient proton hopping, the loss of water molecules at temperatures above 70 °C limited its working conditions.

Among the sulfonic acid/sulfonate group-containing Cu-MOFs reviewed (summarized in Table 3), two frameworks showed high proton conductivity ($>10^{-3}$ S cm^{-1}): the mixed-linker $[\{Cu_2(sba)_2(bpg)_2(H_2O)_3\}\cdot 5H_2O]_n$ (sba = 4-sulfobenzoate, bpg = bipyridine glycoluril) and tetranuclear copper-cluster Cu-DSOA (DSOA = 2,2′-disulfonate-4,4″-oxydibenzoic acid). Both frameworks contained a high number of water molecules per asymmetric unit, indicating strong water dependence for proton conductivity. Furthermore, high proton conductivity was maintained for over 12 hours in the mixed-linker MOF under high temperatures and humidity conditions, with its structural stability confirmed by PXRD. Conversely, Cu-DSOA partially lost crystallinity after standard impedance measurements, revealing less structural stability.

2.4. Composites with acid-functionalized polymers

While highly ordered structures provide a deep understanding of the underlying mechanisms of proton conduction, they have limitations in the performance of proton conductivity when incorporated into practical applications. Grain boundaries in MOF microcrystallites and MOF-polymer mixed matrices can disrupt proton conduction channels, thus diminishing the material's potential conductivity. By contrast, the incorporation of a polymer with acidic groups can help bridge these grain boundaries and enhance proton conductivity.

Mahimai and colleagues explored Cu-MOF-polymer composites using 2,6-naphthalene dicarboxylic acid as an organic linker.[83] They used polystyrene as the composite material but added a sulfonate group to the polymer to increase acidity and, thereby, proton conductivity (Fig. 9(a)). This composite material achieved a maximum conductivity of 1.65×10^{-2} S cm^{-1}. Additionally, they further enhanced proton conductivity to 3.1×10^{-2} S cm^{-1} by casting the MOF with additional ligands, specifically 1,2-dimethyl-3-propylimidazolium iodide. This study demonstrates the importance of selecting appropriate composite materials to improve proton conductivity.

Another strategy involves incorporating the polymer directly into the MOF pores to enable direct interactions between the MOF's organic linkers and the polymer. Li and coauthors synthesized a Cu-MOF with a sulfonate-imidazolium ion pair inside the MOF pores using 1-(1-ethyl-3-imidazolio)-propane-3-sulfonate (MIMS).[84] In addition, they incorporated poly(vinyl alcohol) (PVA), which contains hydroxyl groups that can facilitate proton conduction (Fig. 9(b)). This strategy achieved a maximum conductivity of 2.3×10^{-3} S cm^{-1}, nearly double that of the commercial Nafion-115 (1.25×10^{-3} S cm^{-1}). Furthermore, the activation energy for proton transport was reduced from 0.96 eV to 0.42 eV, indicating a combined Grotthuss and vehicle mechanism for proton transport.

Additionally, disrupting the long-range order without fully transforming the material into an amorphous phase can enhance proton conductivity. Disordered structures, such as metal–organic gel (MOG) materials, present fascinating alternatives due to their numerous defective sites and solvent-absorbing networks, which can potentially improve conductivity.[85,86] Tang and colleagues investigated this approach by reducing the crystallinity of HKUST-1 and, thus, converting it into a MOG-type HKUST-1, which resulted in a mesoporous, low-crystallinity network with deficient N_2 adsorption capacity.[87] At 80 °C under 75% RH, the resulting proton conductivities were 7.2×10^{-5} and 1.15×10^{-3} S cm^{-1} for HKUST-1 and MOG-HKUST-1, respectively, showing that a less ordered three-dimensional network

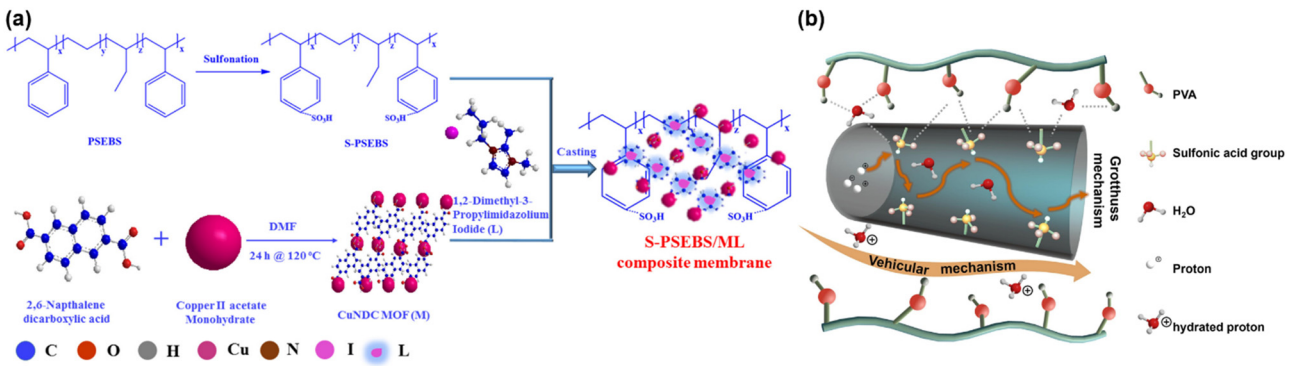

Fig. 9 (a) Schematic representation for preparation of S-PSEBS/ML composite membrane. Reproduced with permission from ref. 83, Copyright 2022, American Chemical Society. (b) The possible proton transport pathways of CL-PVA/Cu-MOF-15. Reproduced with permission from ref. 84, Copyright 2023, Elsevier.

provided an easier proton transfer pathway. However, MOG-type HKUST-1 was unstable and lost its conductivity after only three days.

3. MOF fabrications

In the studies, the conductivity of Cu-MOFs was primarily assessed in the form of compacted pellets of microcrystalline material. However, this method does not adequately represent the actual working conditions of proton-exchange membrane fuel cells (PEMFCs). It restricts a proper evaluation of the performance of Cu-MOFs as components of PEMs. Typically obtained as microcrystalline powders, Cu-MOFs face challenges such as limited proton transfer over long distances due to grain boundaries, and their brittle nature prevents them from forming films independently, which limits their application as solid-state electrolytes in fuel cells.

To be effectively integrated into PEMs, Cu-MOFs should be able to produce a uniform and durable film or be well-dispersed in a membrane. Different strategies have been developed to address this challenge, such as depositing Cu-MOFs as thin films on a conductive substrate or integrating Cu-MOFs into membranes to create mixed-matrix membranes. Relevant studies concerning these strategies are discussed in the following sections.

3.1. Thin films

In 2014, Qi and coauthors achieved the *in situ* growth of a micron-thick (~0.15 μm) dense HKUST-1 film on a copper foil under mild conditions.[88] The resulting film exhibited a conductivity of 0.69×10^{-3} S cm^{-1} after exposal for three days at 98% RH, which was an order of magnitude higher than the microcrystalline HKUST-1 reported by Jeong in 2012.[57] However, the activation energy for this HKUST-1 microfilm was not reported.

Given the promising proton conduction performance of NENU-3, a derivative of HKUST-1 encapsulating the polyoxometalate $[PW_{12}O_{40}]^{3-}$, several studies have explored the electrochemical thin film fabrication of this material with controlled crystallite size and thickness.[89,90] Zhang and collaborators investigated the proton conductivity of a 12-μm-thick NENU-3 film, finding that its conductivity was negligible as-synthesized but increased substantially to 2.9×10^{-5} S cm^{-1} at 40 °C under 97% RH after humidification for 3 days. For comparison, an HKUST-1 film grown using the same methodology exhibited a maximum conductivity of 1.8×10^{-6} S cm^{-1} at 35 °C under 97% RH. The activation energy for the NENU-3 film was estimated to be 0.38 eV, significantly lower than the activation energy of 0.61 eV for the pristine HKUST-1, suggesting that the POM clusters are critical proton carriers whose solvation depends on temperature.

Smart materials responding to external stimuli such as light are highly desirable for various applications, including remote control of fundamental material properties.[91] Two notable studies focused on controlling the reversible conductivity of composite materials through light irradiation. The first involved azobenzene derivatives that can switch *trans*-to-*cis* isomerization under UV light and *cis*-to-*trans* back-isomerization with thermal treatment. In 2018, Müller and coauthors grew a film of $Cu_2(F_2AzoBDC)_2(dabco)$ ($F_2AzoBDC$ = (*E*)-2-((2,6-difluorophenyl)diazenyl)terephthalate, dabco = 1,4-diazabicyclo[2.2.2]octane) on a quartz substrate, subsequently loading it with 1,4-butanediol or 1,2,3-triazole (Fig. 10(a)).[92] When the film was virtually empty, it exhibited negligible proton conduction in either the *cis*- or *trans*-form at 25 °C. However, when loaded with guest molecules, such as 1,4-butanediol or 1,2,3-triazole, conductivity was much enhanced in the *trans*-form, reaching up to 1.24×10^{-4} S cm^{-1} for 1,2,3-triazole@$Cu_2(F_2AzoBDC)_2$(dabco). Conductivity could be switched between 7.9×10^{-5} S cm^{-1} (*cis*) and 1.24×10^{-4} S cm^{-1} (*trans*) by irradiating green light (530 nm) and violet (400 nm), respectively (Fig. 10(b)).

In another study, Wang and coauthors prepared an HKUST-1 membrane using a solid confined conversion process.[93] Due to HKUST-1's intrinsic photothermal properties, the authors evaluated the membrane's conductivity in the dark at 55 °C under 95% RH (1.35×10^{-4} S cm^{-1}), which significantly dropped to 2.27×10^{-7} S cm^{-1} under a Xe lamp at 0.5 sun intensity. Remarkably, conductivity could be restored to its initial value by returning the membrane to darkness (Fig. 10(c)). This behavior was attributed to the loss of pore-filling water molecules due to local heating effects from the photothermal properties of HKUST-1 when exposed to light. Furthermore, the membrane showed better proton conductivity than pelletized microcrystalline HKUST-1 under similar conditions (Fig. 10(d)).

Pelletized powder materials generally exhibit lower conductivity compared to the thin films reported in these studies, as summarized in Table 4. Among them, the HKUST-1 microfilm reported by Qi and colleagues achieved the highest conductivity (10^{-4} S cm^{-1}). This comparison highlights the significant influence of the deposition method on the films' conductivities. For example, the 0.15 μm-thick HKUST-1 thin film produced by using a mother solution deposition technique demonstrated ~383 times higher conductivity compared to a (10 times thicker) film synthesized *via* a solid confined conversion process and showed 5 times higher conductivity than one (0.12 μm thick) created using an electrochemical method. However, to achieve the maximum conductivity of 10^{-4} S cm^{-1}, the HKUST-1 microfilm required three days of exposure to humid conditions (98% RH at 25 °C) to ensure adequate water retention within its pores. Furthermore, although these thin films are characterized as dense, individual crystallite grains are still distinguishable, suggesting that grain boundaries may substantially hinder proton conductivity. Therefore, developing more uniform Cu-MOF thin films is essential to enhance the conductivity further.

3.2. Mixed-matrix membranes

Among Cu-based MOFs, HKUST-1 is considered a benchmark material for studying proton conductivity due to its paddlewheel-like dimeric Cu units linked by trimesic acid (benzene-1,3,5-tricarboxylate) anions. Also, the ease of its synthesis on a gram scale from inexpensive chemicals has made it

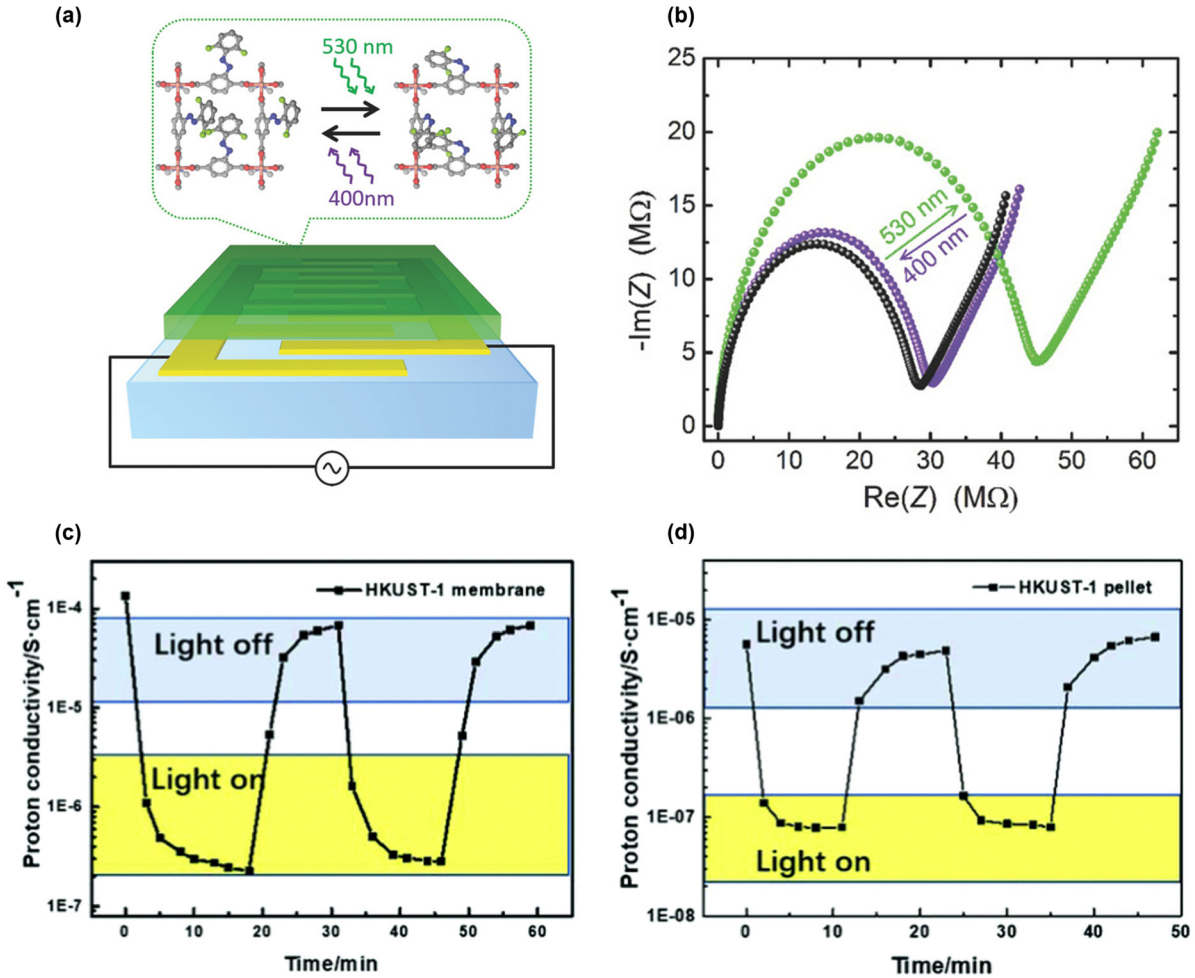

Fig. 10 (a) Schematization of surface mounted $Cu_2(F_2AzoBDC)_2(dabco)$ film: $Cu_2(F_2AzoBDC)_2(dabco)$ is the green layer on the interdigitated gold electrodes (yellow layer) on quartz substrate (light blue layer). $Cu_2(F_2AzoBDC)_2(dabco)$ structure viewed along the [001] direction. Black lines show the connection to the electric circuit and the impedance spectrometer. Representation of photoswitching between *cis*- and *trans*-fluorinated azobenzene side groups in $Cu_2(F_2AzoBDC)_2(dabco)$ when irradiated by green light (530 nm from *trans* to *cis*) and with violet light (400 nm from *cis* to *trans*). (b) Nyquist plot of the impedance of triazole@$Cu_2(F_2AzoBDC)_2(dabco)$. The black data is measured in the pristine sample (*trans*), green after irradiation with green light (*cis*), and violet after irradiation with violet light (*trans*). Reproduced with permission from ref. 92, Copyright 2018, Wiley, VCH. (c) and (d) Proton conductivity changes of the HKUST-1 (c) membrane and (d) pellet with and without light at 55 °C under 95% RH. Reproduced with permission from ref. 93, Copyright 2021, Royal Society of Chemistry.

Table 4 Summary of proton-conductivities of Cu-MOFs thin films

Material	Thickness (μm)	σ (S cm^{-1})	E_a (eV)	Temperature (°C)	% RH	Ref.
HKUST-1 microfilm	0.15	6.9×10^{-4}	NR	25	98	88
1,2,3-Triazole@$Cu_2(F_2AzoBDC)_2(dabco)$	0.15	1.24×10^{-4}	NR	25	NR	92
HKUST-1 membrane	1.5	1.35×10^{-4}	NR	55	95	93

the most studied Cu-MOF as a filler for mixed-matrix membranes. In an early study, Kim and colleagues incorporated various amounts of HKUST-1 into Nafion to enhance its conductivity.[94] The membranes were prepared using a solution casting method, and acids were fed into them by soaking them in a 50 wt% H_3PO_4 solution. While water uptake by the membranes decreased with increasing HKUST-1 content, the maximum acid uptake occurred with the 2.5 wt% content of HKUST-1. The acid-doped 2.5 wt% HKUST-1/Nafion membrane exhibited the highest conductivity, 1.8×10^{-2} S cm^{-1} at 25 °C under 100% RH.

More recently, Li and collaborators investigated the proton-conducting properties of two $Cu_{12}S_6$-cluster-based MOFs incorporated into Nafion.[95] The respective conductivities were found to be 3.63×10^{-5} and 2.75×10^{-5} S cm^{-1} for $[Cu_{12}(MES)_6(H_2O)_3]_n$ and $([Cu_{12}(MPS)_6(H_2O)_4]\cdot 6H_2O)_n$ (H_2MES = 2-mercaptoethanesulfonate acid, H_2MPS = 2-mercaptopropanesulfonate acid) at 60 °C under 98% RH, with activation energies of 0.12 eV and 0.22 eV,

respectively. The differences in proton conductivities were attributed to structural variations between the MOFs: $[Cu_{12}(MES)_6(H_2O)_3]_n$ contained one additional partially coordinated μ_2-SO_3 group per asymmetric unit, making it more acidic than $[Cu_{12}(MPS)_6(H_2O)_4]$. Moreover, although $[Cu_{12}(MES)_6(H_2O)_3]_n$ had fewer water molecules per copper unit, these molecules were firmly coordinated to the Cu centers, forming a more ordered H-bond network, thereby facilitating easier proton transport.

Nafion is known for its high methanol permeability, which can adversely affect DMFC performance.[96,97] Alternative sulfonated polymers, such as SPEEK, have been investigated to mitigate methanol crossover. However, even SPEEK-based composites have exhibited low stability and conductivity at elevated temperatures.[98,99] Consequently, HKUST-1 has also been studied as a filler in SPEEK-based MMMs. In a 2018 study, Niluroutu and coworkers dispersed HKUST-1 varying its amount (1, 2, 3, and 5 wt%) into SPEEK to form composite membranes, each approximately 170 μm thick, denoted as SP/CT-MOF-*n*, where *n* represents the Cu-MOF contents (wt%) in the membrane.[100] Proton incorporation was achieved by loading H_2SO_4 groups into the prepared membranes. The composite with 3 wt% HKUST-1 (SP/CT-MOF-3) exhibited the highest conductivity (4.5×10^{-2} S cm^{-1}) at 70 °C under 98% RH and the lowest activation energy (0.08 eV) among the prepared membranes. The carboxylate groups in HKUST-1 contributed to better connectivity for the ionic channels of SPEEK by forming H-bonds with the sulfonic groups of SPEEK, as illustrated in Fig. 11(a). The inclusion of 3 wt% HKUST-1 reduced methanol permeability to nearly half (4.26×10^{-7} cm^2 s^{-1}) compared to pristine SPEEK (7.95×10^{-7} cm^2 s^{-1}) due to the strong interaction of methanol molecules with HKUST-1, while the sulfonic groups in the SPEEK facilitated hydronium ion transport. The electrochemical selectivity, defined as the ratio between conductivity and methanol permeability, was estimated for the prepared composite materials, with SP/CT-MOF-3 showing the highest value ($\sim 1.1 \times 10^5$ S cm^{-3} s).

Further advancing this approach, Hu and collaborators prepared a hybrid material by combining HKUST-1 and boron phosphate (BPO_4), an inorganic compound known for its ability to retain water molecules up to 300 °C owing to the strong H-bonds formed between water molecules and boron or phosphorus.[101] The resulting HKUST-1/BPO_4 hybrid materials (HB) were dispersed in SPEEK membranes for DMFC applications. The amount of HKUST-1 in the SPEEK was kept constant, while the BPO_4 content 5, 10, 15, 20 wt% relative to HKUST-1, named as HB-5, HB-10, HB-15, HB-20, respectively. Increasing BPO_4 content improved methanol permeability, oxidative stability, and mechanical strength while reducing area by polymeric swelling compared to pristine SPEEK. All composite membranes showed higher conductivity than pristine SPEEK, with the highest conductivity (3.74×10^{-2} S cm^{-1}) at 80 °C under 100% RH and the lowest activation energy (0.09 eV) reported for the sample containing 10 wt% BPO_4. Further increased BPO_4 content made the proton transport path more tortuous, resulting in lower conductivity and higher activation energy, as depicted in Fig. 11(b) and (c).

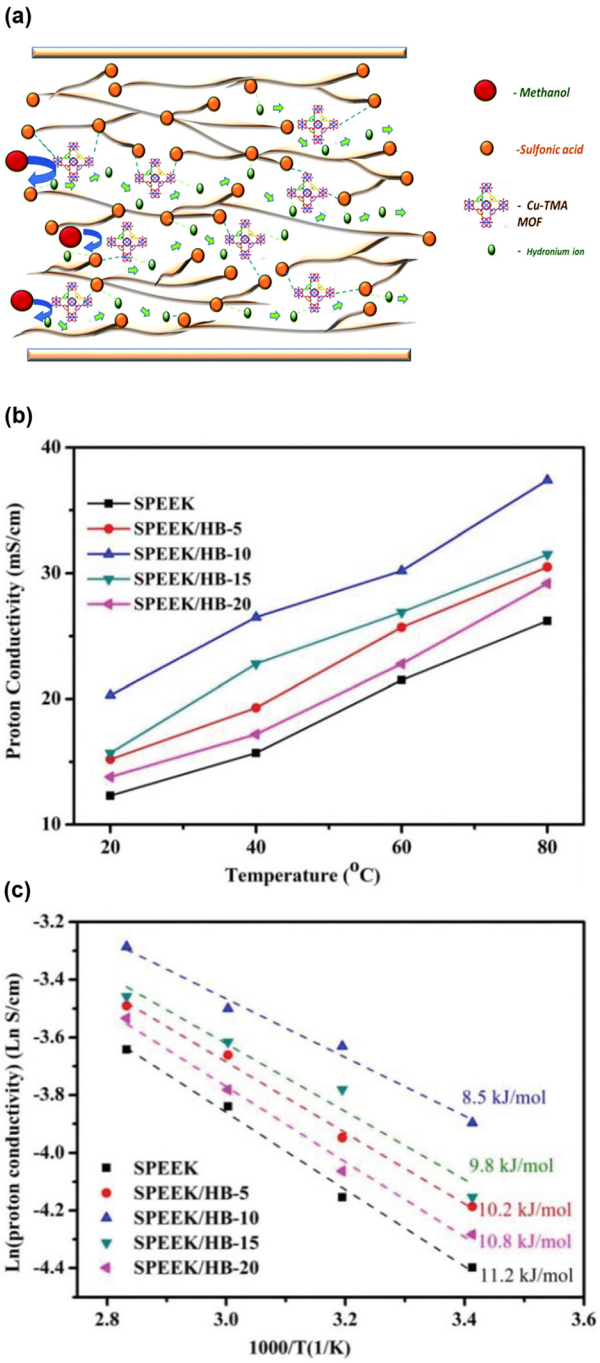

Fig. 11 (a) Illustration of HKUST-1 in sPEEK matrix, SP/CT-MOF-3, depicting hydrogen bond network, proton transport pathways and low methanol permeability. Reproduced with permission from ref. 100, Copyright 2018, Royal Society of Chemistry. (b) Proton conductivity and (c) Arrhenius plots of pristine SPEEK and HKUST-1/BPO_4 in sPEEK matrix. Reproduced with permission from ref. 101, Copyright 2021, Wiley VCH.

Biopolymer-based PEMs have gained attention for their high availability, non-toxicity, and abundance of active functional groups.[102–104] Chitosan, in particular, has been highlighted for DMFC applications due to its rigid structure, crystallinity, and hydrophilicity, attributed to its amine, hydroxyl, and ether functional groups.[105,106] Divya and coauthors fabricated sulfonated

Table 5 Summary of proton-conductivities of MMM comprised of Cu-MOFs

Material	Polymer	σ (S cm^{-1})	E_a (eV)	Temperature (°C)	% RH	Ref.
2.5 wt% HKUST-1/Nafion	Nafion	1.8×10^{-2}	NR	25	100	94
$[Cu_{12}(MES)_6(H_2O)_3]_n$/Nafion	Nafion	3.63×10^{-5}	0.12	60	98	95
$[\{Cu_{12}(MPS)_6(H_2O)_4\}\cdot 6H_2O]_n$/Nafion	Nafion	2.75×10^{-5}	0.22	60	98	95
SP/CT-MOF-3	SPEEK	4.5×10^{-2}	0.08	70	98	100
SPEEK/HB-10	SPEEK	3.74×10^{-2}	0.09	80	100	101
S-Chitosan-0.5	Sulfonated chitosan	6.19×10^{-3}	NA	80	NA	107
MMM-4	PVP/PVDF	8.0×10^{-4}	0.19	80	98	111
Cu-MOF@PP-50	PVP/PVDF	4.36×10^{-4}	0.09	80	98	112

chitosan membranes incorporating HKUST-1 as a filler in varying amounts (0.25, 0.5, or 1 wt% relative to chitosan).[107] The 0.5 wt% HKUST-1 composite, designated as S-Chitosan-0.5, showed the best conductivity (6.19×10^{-3} S cm^{-1}) at 80 °C, lower methanol permeability (3.01×10^{-8} cm^2 s^{-1}), and higher membrane selectivity (1.78×10^5 S cm^{-3} s). Although the maximum conductivity achieved in this study was lower than that reported for SP/CT-MOF-3, the membrane selectivity of S-chitosan-0.5 was higher.

Poly(vinylpyrrolidone) (PVP) and poly(vinylidene fluoride) (PVDF) blends have been explored as alternatives for high-temperature PEMFCs.[108–110] Moi and coworkers prepared PVP/PVDF membranes incorporating different amounts of Cu-SAT, $[\{Cu_2(\mu_2\text{-}OH)_2(NDS)(T4A)_2\}\cdot 2DMF]_n$ (H_2NDS = 1,5-naphthalenedisulfonic acid, T4A = 1,2,4-triazol-4-amine), a MOF containing sulfonate and amine groups.[111] They found that the maximum amount of Cu-SAT effectively integrated into the membrane was 60 wt% (designated as MMM-4). Among the prepared membranes, MMM-4 demonstrated a 52% increase in conductivity (8×10^{-4} S cm^{-1}) at 80 °C under 98% RH and a 20% reduction in activation energy (0.187 eV) compared to the pristine Cu-SAT. They found that the time-dependent conductivity of MMM-4 remained nearly unchanged even for five days, indicating its potential for practical applications. In a subsequent study conducted in 2022, Bao and collaborators developed PVP/PVDF composite membranes with an increased loading of up to 50 wt% of $[Cu(BTTA)H_2O]_n\cdot 6nH_2O$ (BTTA = 2,5-bis(1,2,4-triazol-1-yl)terephthalate).[112] The membrane containing 50 wt% MOF (Cu-MOF@PP-50) exhibited the highest conductivity and lowest activation energy among the prepared membranes, achieving 4.36×10^{-4} S cm^{-1} at 80 °C under 98% RH with an activation energy of 0.09 eV. This result represents a two-order magnitude increase in conductivity compared to pristine $[Cu(BTTA)H_2O]_n\cdot 6nH_2O$ and an 11-fold increase compared to the bare PVP/PVDF membrane. While PVP/PVDF composite membranes have been investigated as candidates for high-temperature PEMFCs (intended to operate between 120 °C and 200 °C), they have only been tested up to 80 °C. Therefore, evaluating these materials at higher temperatures is crucial to verify their suitability for such applications. Moreover, compared to MMMs made from other polymers, the proton conductivity of PVP/PVDF composite membranes is at least one order of magnitude lower, even with a lower MOF content (*vice versa*, a higher polymer content). Given their high chemical stability, proton activation *via* soaking in oxo-acid solutions could enhance performance, but this or other enhancement strategies remain unexplored.

Among the MMMs discussed, those based on Nafion and SPEEK with HKUST-1 fillers exhibited the highest conductivity ($\sim 10^{-2}$ S cm^{-1}), as summarized in Table 5. However, only the SPEEK-based MMMs were tested at high temperatures (SP/CT-MOF-3 and SPEEK/HB-10, at 70 °C and 80 °C, respectively). Notably, SP/CT-MOF-3 evaluated under open circuit voltage conditions (where methanol crossover was maximized) for 50 hours showed better operational stability than pristine SPEEK. In the case of SPEEK/HB-10, its stability was evaluated and then found to be 17% higher than that of pristine SPEEK (up to 332 minutes). Furthermore, its proton conductivity was maintained for over 72 hours.

The MOF-filled MMMs showed modest conductivity levels but consistently exhibited low activation energies (0.22 eV), comparable to those of pristine SPEEK at 90% RH. These findings underscore the potential of Cu-MOFs for MMMs, presenting a promising opportunity to create composite materials with high proton conductivity.

4. Conclusions

This highlight introduces the proton conductivity of Cu-MOFs in different forms: single crystal, microcrystalline powders, thin films, and fillers in mixed-matrix membranes. For single-crystalline and microcrystalline Cu-MOFs, we highlighted diverse approaches explored by various research groups to design or enhance pathways for water-assisted proton transport within Cu-MOF channels. The predominant strategies involved utilizing linkers rich in hydrophilic atoms, such as oxygen, nitrogen, or sulfur; incorporating polyoxometalates (POMs) as integral building units or guests within the pores; and introducing guest molecules capable of forming H-bonds. The use of N-rich linkers, in particular, has led to highly proton-conductive materials, underlining the significance of stable, uninterrupted H-bond networks between the framework and guest molecules to support efficient proton hopping.

Combining multiple strategies to improve proton conductivity, such as adding additional proton carriers (like imidazole) to an already POM-loaded MOF, resulted in a six-order magnitude increase in proton conductivity, even at relatively low humidity levels, making this approach particularly attractive for further exploration. We also interpret the role of guest molecules and

proton carriers in different Cu-MOFs, emphasizing the importance of well-ordered structures to elucidate the relationships between structure and proton transport performance in Cu-MOFs.

Regarding Cu-MOF thin films, most research has focused on synthesizing HKUST-1 thin films, resulting in only moderate proton conductivities, mainly because HKUST-1 inherently exhibits low conductivity. Although further efforts should be made to explore other Cu-MOFs with high proton conductivity in their microcrystalline forms, developing optimized deposition techniques for each Cu-MOF is essential to enhance their performance as thin films.

Cu-MOFs in MMMs represent a relatively underexplored area, offering opportunities for significant advancements. So far, the most effective polymers for these composites have been Nafion and SPEEK, though they come with known limitations. Most studies have concentrated on proton conductivity and activation energy, often neglecting other essential evaluations. Comprehensive assessments are necessary, including not only long-term conductivity but also thermal, chemical, and mechanical stability (especially in response to swelling cycles). Research on optimizing the balance between membrane thickness, conductivity, and fuel crossover will pave the way for more efficient and robust proton-exchange membranes.

The future of Cu-MOFs in fuel cells is promising, particularly as advancements continue to refine their integration into PEMs and explore new methods to enhance their conductivity, stability, and overall performance. By leveraging their unique properties, Cu-MOFs could play a crucial role in developing next-generation energy conversion technologies.

Author contributions

B. J. K., S. H. P. and M. L. D.-R. wrote the original draft. B. J. K. visualized the work. M. L. D.-R. conceptualized the study. N. C. J. supervised all the papers.

Data availability

No primary research results, software or code have been included, and no new data were generated or analysed as part of this review.

Conflicts of interest

There are no conflicts to declare.

Acknowledgements

This work was supported by the Ministry of Science and ICT (MSIT) of Korea under the auspices of the Basic Science Research Program sponsored by the National Research Foundation (RS-2023-NR077060) and by the DGIST R&D Program (25-HRHR+-01).

Notes and references

1 S. Chakraborty, D. Elangovan, K. Palaniswamy, A. Fly, D. Ravi, D. A. S. Seelan and T. K. R. Rajagopal, *Energies*, 2022, **15**, 9520.
2 H. S. Das, C. W. Tan and A. H. M. Yatim, *Renewable Sustainable Energy Rev.*, 2017, **76**, 268–291.
3 L. Venturelli, P. E. Santangelo and P. Tartarini, *Appl. Therm. Eng.*, 2009, **29**, 3469–3475.
4 F.-C. Wang, P.-C. Kuo and H.-J. Chen, *Int. J. Hydrogen Energy*, 2013, **38**, 5845–5856.
5 K. Nikiforow, P. Koski, H. Karimäki, J. Ihonen and V. Alopaeus, *Int. J. Hydrogen Energy*, 2016, **41**, 14952–14970.
6 I. Gatto, A. Saccà, R. Pedicini, E. Passalacqua and A. Carbone, *Int. J. Hydrogen Energy*, 2021, **46**, 27687–27699.
7 Y. Shen, X. Yan, L. An, S. Shen, L. An and J. Zhang, *Appl. Energy*, 2022, **313**, 118781.
8 S. Sun, M. Zhao, Q. Wang, S. Xue, Q. Huang, N. Yu and Y. Wu, *Small*, 2023, 2205835.
9 S. Zou, Y. Li, H. Jin, F. Ning, P. Xu, Q. Wen, S. Pan, X. Dan, W. Li and X. Zhou, *Adv. Energy Mater.*, 2021, **12**, 2103178.
10 M. W. Ellis, M. R. Von Spakovsky and D. J. Nelson, *Proc. IEEE*, 2001, **89**, 1808–1818.
11 J. Lindorfer, D. C. Rosenfeld and H. Böhm, Fuel Cells: Energy Conversion Technology, in *Future Energy*, ed. T. M. Letcher, Elsevier, Amsterdam, 3rd edn, 2020, ch. 23, pp. 495–517.
12 P. Colomban and A. Novak, Proton conductors: classification and conductivity, in *Proton conductors: Solids, membranes and gels – materials and devices*, ed. P. Colomban, Cambridge University Press, Cambridge, 1992, ch. 23, pp. 38–60.
13 J. A. Elliott and S. J. Paddison, *Phys. Chem. Chem. Phys.*, 2007, **9**, 2602–2618.
14 G. A. Ludueña, T. D. Kühne and D. Sebastiani, *Chem. Mater.*, 2011, **23**, 1424–1429.
15 L. Y. Zhu, Y. C. Li, J. Liu, J. He, L. Y. Wang and J. D. Lei, *Pet. Sci.*, 2022, **19**, 1371–1381.
16 Y. Oshiba, J. Tomatsu and T. Yamaguchi, *J. Power Sources*, 2018, **394**, 67–73.
17 Z. Long and K. Miyatake, *iScience*, 2021, **24**, 102962.
18 V. Atanasov, A. Oleynikov, J. Xia, S. Lyonnard and J. Kerres, *J. Power Sources*, 2017, **343**, 364–372.
19 N. Sulaiman, M. A. Hannan, A. Mohamed, E. H. Majlan and W. R. Wan Daud, *Renewable Sustainable Energy Rev.*, 2015, **52**, 802–814.
20 P. Zegers, *J. Power Sources*, 2006, **154**, 497–502.
21 N. E. Wong, P. Ramaswamy, A. S. Lee, B. S. Gelfand, K. J. Bladek, J. M. Taylor, D. M. Spasyuk and G. K. H. Shimizu, *J. Am. Chem. Soc.*, 2017, **139**, 14676–14683.
22 Z. Y. Zhang, G. X. Qin, X. M. Li, H. L. Dong, S. Wan, Y. H. Ni, J. Liu, Z. Q. Chen and Z. Su, *Inorg. Chem.*, 2022, **61**, 15166–15174.
23 S. Mukhopadhyay, J. Debgupta, C. Singh, R. Sarkar, O. Basu and S. K. Das, *ACS Appl. Mater. Interfaces*, 2019, **11**, 13423–13432.
24 M. K. Sarango-Ramirez, J. Park, J. Kim, Y. Yoshida, D. W. Lim and H. Kitagawa, *Angew. Chem., Int. Ed.*, 2021, **60**, 20173–20177.
25 A. Shigematsu, T. Yamada and H. Kitagawa, *J. Am. Chem. Soc.*, 2011, **133**, 2034–2036.
26 A. Mallick, T. Kundu and R. Banerjee, *Chem. Commun.*, 2012, **48**, 8829–8831.
27 V. G. Ponomareva, K. A. Kovalenko, A. P. Chupakhin, D. N. Dybtsev, E. S. Shutova and V. P. Fedin, *J. Am. Chem. Soc.*, 2012, **134**, 15640–15643.
28 F. M. Zhang, L. Z. Dong, J. S. Qin, W. Guan, J. Liu, S. L. Li, M. Lu, Y. Q. Lan, Z. M. Su and H. C. Zhou, *J. Am. Chem. Soc.*, 2017, **139**, 6183–6189.
29 M. Lupa, P. Kozyra and D. Matoga, *ACS Appl. Energy Mater.*, 2023, **6**, 9118–9123.
30 S. Pili, S. P. Argent, C. G. Morris, P. Rought, V. Garcia-Sakai, I. P. Silverwood, T. L. Easun, M. Li, M. R. Warren, C. A. Murray, C. C. Tang, S. Yang and M. Schroder, *J. Am. Chem. Soc.*, 2016, **138**, 6352–6355.
31 J. Chen, Q. Mei, Y. Chen, C. Marsh, B. An, X. Han, I. P. Silverwood, M. Li, Y. Cheng, M. He, X. Chen, W. Li, M. Kippax-Jones, D. Crawshaw, M. D. Frogley, S. J. Day, V. Garcia-Sakai, P. Manuel, A. J. Ramirez-Cuesta, S. Yang and M. Schroder, *J. Am. Chem. Soc.*, 2022, **144**, 11969–11974.

32 S. Kanda, K. Yamashita and K. Ohkawa, *Bull. Chem. Soc. Jpn.*, 2006, **52**, 3296–3301.
33 Y. Nagao, T. Kubo, K. Nakasuji, R. Ikeda, T. Kojima and H. Kitagawa, *Synth. Met.*, 2005, **154**, 89–92.
34 J. Y. Choi, M. Stodolka, N. Kim, H. T. B. Pham, B. Check and J. Park, *Chem*, 2023, **9**, 143–153.
35 M.-Y. Zhang, X.-N. Qin, C.-X. Zhang and Q.-L. Wang, *ACS Appl. Nano Mater.*, 2024, **7**, 7063–7071.
36 H. Huang, Z. Zhong, J. Li and H. Li, *ACS Appl. Energy Mater.*, 2024, **7**, 10804–10814.
37 H. Bunzen, A. Javed, D. Klawinski, A. Lamp, M. Grzywa, A. Kalytta-Mewes, M. Tiemann, H.-A. K. von Nidda, T. Wagner and D. Volkmer, *ACS Appl. Nano Mater.*, 2019, **2**, 291–298.
38 W. M. Haynes, *CRC Handbook of Chemistry and Physics*, CRC Press, Boca Raton, FL, 2016–2017.
39 Y. Chen, Y. Zhang, Q. Huang, X. Lin, A. Zeb, Y. Wu, Z. Xu and X. Xu, *ACS Appl. Energy Mater.*, 2022, **5**, 7842–7873.
40 C. Kong, G. Jiang, Y. Sheng, Y. Liu, F. Gao, F. Liu and X. Duan, *Chem. Eng. J.*, 2023, **460**, 141803.
41 R. Singh, G. Singh, N. George, G. Singh, S. Gupta, H. Singh, G. Kaur and J. Singh, *Catalysts*, 2023, **13**, 130.
42 J. E. Cun, X. Fan, Q. Pan, W. Gao, K. Luo, B. He and Y. Pu, *Adv. Colloid Interface Sci.*, 2022, **305**, 102686.
43 S. Kanda, K. Yamashita and K. Ohkawa, *Bull. Chem. Soc. Jpn.*, 1979, **52**, 3296–3301.
44 Y. Nagao, M. Fujishima, R. Ikeda, S. Kanda and H. Kitagawa, *Synth. Met.*, 2003, **133–134**, 431–432.
45 Y. Nagao, T. Kubo, K. Nakasuji, R. Ikeda, T. Kojima and H. Kitagawa, *Synth. Met.*, 2005, **154**, 89–92.
46 Y. Zhou, J. Yang, H. Su, J. Zeng, S. P. Jiang and W. A. Goddard, *J. Am. Chem. Soc.*, 2014, **136**, 4954–4964.
47 W. J. Liu, L. Z. Dong, R. H. Li, Y. J. Chen, S. N. Sun, S. L. Li and Y. Q. Lan, *ACS Appl. Mater. Interfaces*, 2019, **11**, 7030–7036.
48 N. Ogiwara, T. Iwano, T. Ito and S. Uchida, *Coord. Chem. Rev.*, 2022, **462**, 214524.
49 M. L. Wei, J. J. Sun and X. Y. Duan, *Eur. J. Inorg. Chem.*, 2013, 345–351.
50 C. Dey, T. Kundu and R. Banerjee, *Chem. Commun.*, 2012, **48**, 266–268.
51 M. Wei, X. Wang and X. Duan, *Chem. – Eur. J.*, 2013, **19**, 1607–1616.
52 R.-T. Zhang, H.-P. Xiao, Z. Li, M. Wang, Y.-F. Xie, Y.-D. Ye, X.-X. Li and S.-T. Zheng, *CrystEngComm*, 2021, **23**, 2973–2981.
53 M. Wei, L. Chen and X. Duan, *J. Coord. Chem.*, 2014, **67**, 2809–2819.
54 H.-J. Lun, Z.-M. Zhang, Y.-H. Sun, M.-M. Wang, J.-J. Cai, X.-Y. Liang, Y.-M. Li and Y. Bai, *Inorg. Chem.*, 2023, **62**, 17093–17101.
55 Y. Liu, X. Yang, J. Miao, Q. Tang, S. Liu, Z. Shi and S. Liu, *Chem. Commun.*, 2014, **50**, 10023–10026.
56 Y. Ye, W. Guo, L. Wang, Z. Li, Z. Song, J. Chen, Z. Zhang, S. Xiang and B. Chen, *J. Am. Chem. Soc.*, 2017, **139**, 15604–15607.
57 N. C. Jeong, B. Samanta, C. Y. Lee, O. K. Farha and J. T. Hupp, *J. Am. Chem. Soc.*, 2012, **134**, 51–54.
58 S. Khatua, A. Kumar Bar and S. Konar, *Chem. – Eur. J.*, 2016, **22**, 16277–16285.
59 Z. Zhang, Q. Han, S. Zhang, X. Guo, H. Huang, F. Yang and C. Zhong, *ACS Sustainable Chem. Eng.*, 2022, **10**, 11867–11874.
60 B. Gil-Hernández, S. Savvin, G. Makhloufi, P. Núñez, C. Janiak and J. Sanchiz, *Inorg. Chem.*, 2015, **54**, 1597–1605.
61 B. Gil-Hernández, S. Millan, I. Gruber, M. Quirós, D. Marrero-López, C. Janiak and J. Sanchiz, *Inorg. Chem.*, 2022, **61**, 11651–11666.
62 T. Grancha, J. Ferrando-Soria, J. Cano, P. Amorós, B. Seoane, J. Gascon, M. Bazaga-García, E. R. Losilla, A. Cabeza, D. Armentano and E. Pardo, *Chem. Mater.*, 2016, **28**, 4608–4615.
63 R. Li, S. H. Wang, X. X. Chen, J. Lu, Z. H. Fu, Y. Li, G. Xu, F. K. Zheng and G. C. Guo, *Chem. Mater.*, 2017, **29**, 2321–2331.
64 Y. B. Lu, Y. Q. Liao, L. Dong, S. D. Zhu, H. R. Wen, J. Huang, X. X. Dai, P. Lian, X. M. Jiang, R. Li and Y. R. Xie, *Chem. Mater.*, 2021, **33**, 7858–7868.
65 Y. W. You, C. Xue, Z. F. Tian, S. X. Liu and X. M. Ren, *Dalton Trans.*, 2016, **45**, 7893–7899.
66 J. M. Taylor, R. K. Mah, I. L. Moudrakovski, C. I. Ratcliffe, R. Vaidhyanathan and G. K. Shimizu, *J. Am. Chem. Soc.*, 2010, **132**, 14055–14057.
67 Q. Tang, Y. Liu, S. Liu, D. He, J. Miao, X. Wang, G. Yang, Z. Shi and Z. Zheng, *J. Am. Chem. Soc.*, 2014, **136**, 12444–12449.
68 Z.-Y. Ruan, Y.-B. Liang, S.-L. Tan, Y.-X. Tang, W.-Q. Lin, J.-Z. Wu and Y.-C. Ou, *Chem. – Asian J.*, 2021, **16**, 931–936.
69 S. B. Tayade, V. M. Dhavale, A. S. Kumbhar, S. Kurungot, P. Lönnecke, E. Hey-Hawkins and B. Pujari, *Dalton Trans.*, 2017, **46**, 6968–6974.
70 Z. Sun, S. Yu, L. Zhao, J. Wang, Z. Li and G. Li, *Chem. – Eur. J.*, 2018, **24**, 10829–10839.
71 W. Chen, C. Yang, S. Yu, Z. Li and G. Li, *Polyhedron*, 2019, **158**, 377–385.
72 Z.-B. Sun, Y.-L. Li, Z.-H. Zhang, Z.-F. Li, B. Xiao and G. Li, *New J. Chem.*, 2019, **43**, 10637–10644.
73 M. E. Scofield, H. Liu and S. S. Wong, *Chem. Soc. Rev.*, 2015, **44**, 5836–5860.
74 J. P. Guthrie, *Can. J. Chem.*, 1978, **56**, 2342–2354.
75 H. Dong, H. Du, S. R. Wickramasinghe and X. Qian, *J. Phys. Chem. B*, 2009, **113**, 14094–14101.
76 X. Y. Dong, R. Wang, J. B. Li, S. Q. Zang, H. W. Hou and T. C. W. Mak, *Chem. Commun.*, 2013, **49**, 10590–10592.
77 X. Meng, S. Y. Song, X. Z. Song, M. Zhu, S. N. Zhao, L. L. Wu and H. J. Zhang, *Chem. Commun.*, 2015, **51**, 8150–8152.
78 S. B. Tayade, R. Illathvalappil, V. Lapalikar, D. Markad, S. Kurungot, B. Pujari and A. S. Kumbhar, *Dalton Trans.*, 2019, **48**, 11034–11044.
79 G. Zhang and H. Fei, *Chem. Commun.*, 2017, **53**, 4156–4159.
80 H. G. Yu, B. Li, S. Liu, C. Jiang, Y. S. Li, Y. P. Wu, J. Zhao and D. S. Li, *J. Solid State Chem.*, 2021, **294**, 121860.
81 R. Moi, A. Ghorai, S. Banerjee and K. Biradha, *Cryst. Growth Des.*, 2020, **20**, 5557–5563.
82 M. Rautenberg, B. Bhattacharya, C. Das and F. Emmerling, *Inorg. Chem.*, 2022, **61**, 10801–10809.
83 B. M. Mahimai, G. Sivasubramanian, S. Moorthy and P. Deivanayagam, *Ind. Eng. Chem. Res.*, 2022, **61**, 8081–8090.
84 Z. Li, Y. Zhou, J. Hu, C. Shi, S. Liu, Y. Ge, T. Zhou and Y. Ye, *Chem. Eng. J.*, 2024, **480**, 148146.
85 D. Gao, J. Tang, F. Zhang, C. Wen, L. Feng, C. Wan, F. Qu and X. Liang, *J. Colloid Interface Sci.*, 2023, **650**, 19–27.
86 S. Ma, J. Xu, S. Sohrabi and J. Zhang, *J. Mater. Chem. A*, 2023, **11**, 11572–11606.
87 H. Tang, X. Lv, J. Du, Y. Liu, J. Liu, L. Guo, X. Zheng, H. Hao and Z. Liu, *Appl. Organomet. Chem.*, 2022, **36**, e6777.
88 Y. Qi, S. Lin, C. Chen, Y. Liu, Z. Qiao, X. Kuang, Q. Su and H. Y. Chao, *J. Mater. Chem. A*, 2014, **2**, 8849–8853.
89 L. Yang, H. Naruke and T. Yamase, *Inorg. Chem. Commun.*, 2003, **6**, 1020–1024.
90 C. Y. Sun, S. X. Liu, D. D. Liang, K. Z. Shao, Y. H. Ren and Z. M. Su, *J. Am. Chem. Soc.*, 2009, **131**, 1883–1888.
91 C. L. Jones, A. J. Tansell and T. L. Easun, *J. Mater. Chem. A*, 2016, **4**, 6714–6723.
92 K. Muller, J. Helfferich, F. Zhao, R. Verma, A. B. Kanj, V. Meded, D. Bleger, W. Wenzel and L. Heinke, *Adv. Mater.*, 2018, **30**, 1706551.
93 S. Wang, P. Li, S. Fan, Z. Fang, X. Wang, Z. Li and X. Peng, *Dalton Trans.*, 2021, **50**, 2731–2735.
94 H. J. Kim, K. Talukdar and S. J. Choi, *J. Nanopart. Res.*, 2016, **18**, 47.
95 J. M. Li, T. Y. Xu, Y. L. Zhao, X. L. Hu and K. H. He, *Dalton Trans.*, 2021, **50**, 7484–7495.
96 A. V. da Rosa and J. C. Ordóñez, in *Fundamentals of Renewable Energy Processes*, ed. A. V. da Rosa and J. C. Ordóñez, Academic Press, Oxford, 4th edn, 2022, pp. 317–417.
97 F. Samimi and M. R. Rahimpour, in *Methanol*, ed. A. Basile and F. Dalena, Elsevier, 2018, pp. 381–397.
98 G. Chen, L. Ge, J. H. Lee, Z. Zhu and H. Wang, *Matter*, 2022, **5**, 2031–2053.
99 A. Al-Ahmed, A. S. Sultan and S. M. J. Zaidi, in *Ion Exchange Technology I: Theory and Materials*, ed. Inamuddin and M. Luqman, Springer, Netherlands, Dordrecht, 2012, ch. 12, pp. 437–451.
100 N. Niluroutu, K. Pichaimuthu, S. Sarmah, P. Dhanasekaran, A. Shukla, S. M. Unni and S. D. Bhat, *New J. Chem.*, 2018, **42**, 16758–16765.
101 F. Hu, F. Zhong, J. Wang, T. Qu, J. Ni, G. Zheng, C. Gong and H. Liu, *Macromol. Mater. Eng.*, 2021, **306**, 2100053.
102 S. Li, G. Cai, S. Wu, A. Raut, W. Borges, P. R. Sharma, S. K. Sharma, B. S. Hsiao and M. Rafailovich, *Int. J. Mol. Sci.*, 2022, **23**, 15245.
103 M. T. Musa, N. Shaari, S. K. Kamarudin and W. Y. Wong, *Int. J. Energy Res.*, 2022, **46**, 16178–16207.
104 N. Shaari and S. K. Kamarudin, *Polym. Test.*, 2020, **81**, 106183.

105 M. Purwanto, L. Atmaja, M. A. Mohamed, M. T. Salleh, J. Jaafar, A. F. Ismail, M. Santoso and N. Widiastuti, *RSC Adv.*, 2016, **6**, 2314–2322.
106 K. N. Lupatini, J. V. Schaffer, B. Machado, E. S. Silva, L. S. N. Ellendersen, G. I. B. Muniz, R. J. Ferracin and H. J. Alves, *J. Polym. Environ.*, 2018, **26**, 2964–2972.
107 K. Divya, M. S. Sri Abirami Saraswathi, A. Nagendran and D. Rana, *J. Appl. Polym. Sci.*, 2022, **139**, e52829.
108 Z. Guo, X. Xu, Y. Xiang, S. Lu and S. P. Jiang, *J. Mater. Chem. A*, 2015, **3**, 148–155.
109 T. Wen, Z. Shao, H. Wang, Y. Zhao, Y. Cui and H. Hou, *Inorg. Chem.*, 2021, **60**, 18889–18898.
110 L. Sun, Q. Gu, H. Wang, J. Yu and X. Zhou, *RSC Adv.*, 2021, **11**, 29527–29536.
111 R. Moi, A. Ghorai, S. Banerjee and K. Biradha, *Cryst. Growth Des.*, 2020, **20**, 5557–5563.
112 Y. L. Bao, J. Y. Zheng, H. P. Zheng, G. D. Qi, J. R. An, Y. P. Wu, Y. L. Liu, W. W. Dong, J. Zhao and D. S. Li, *J. Solid State Chem.*, 2022, **310**, 123070.